INTERNATIONAL JOURNAL FOR NUMERICAL METHODS IN ENGINEERING
Int. J. Numer. Meth. Engng 2007; **70**:445–495
Published online 17 October 2006 in Wiley InterScience (www.interscience.wiley.com). DOI: 10.1002/nme.1888

Analytical integrations and SIFs computation in 2D fracture mechanics

A. Salvadori[1,*,†] and L. J. Gray[2]

[1]*Dipartimento di Ingegneria Civile, Università di Brescia, via Branze 38, 25123 Brescia, Italy*
[2]*Computer Science and Mathematical Division, Oak Ridge National Laboratory, OakRidge, TN 37831, U.S.A.*

SUMMARY

Analytical integrations, in the framework of linear elastic problems modelled by means of boundary integral equations, have been considered in a previous publication (*Int. J. Numer. Methods Eng.* 2002; **53**(7):1695–1719): the present note aims at extending the subject to linear elastic fracture mechanics. In such a context, special shape functions have been recently proposed (*SIAM J. Appl. Math.* 1998; **58**: 428–455) in order to increase accuracy in stress intensity factors approximation: the closed form solution for 'integrals' that arise from the boundary element method is a goal of the present work. Exploiting the analytical integrations, asymptotical analysis around the crack tip are made possible, with the purpose of formulating a coherent and accurate correlation between approximated stress intensity factors and crack opening displacements over the crack tip straight special elements. Copyright © 2006 John Wiley & Sons, Ltd.

Received 23 February 2006; Revised 14 July 2006; Accepted 18 August 2006

KEY WORDS: fracture mechanics; stress intensity factors; integral equations; boundary elements

1. INTRODUCTION

Modelling linear elastic fracture mechanics (LEFM) problems by means of boundary integral equations (BIEs) and approximating their solution through boundary element methods (BEM) [1] is firmly established in the academic community as well as in industry, as the BEM emerged as the most efficient in simulating crack growth and predicting crack propagation, for being the most accurate method for the numerical evaluation of stress intensity factors (SIFs). Notwithstanding the enormous amount of scientific publications on the subject [2], theoretical and numerical

*Correspondence to: A. Salvadori, Dipartimento di Ingegneria Civile, Università di Brescia, via Branze 38, 25123 Brescia, Italy.
†E-mail: alberto.salvadori@ing.unibs.it

Contract/grant sponsor: Italian Ministry of University and Research (MIUR)

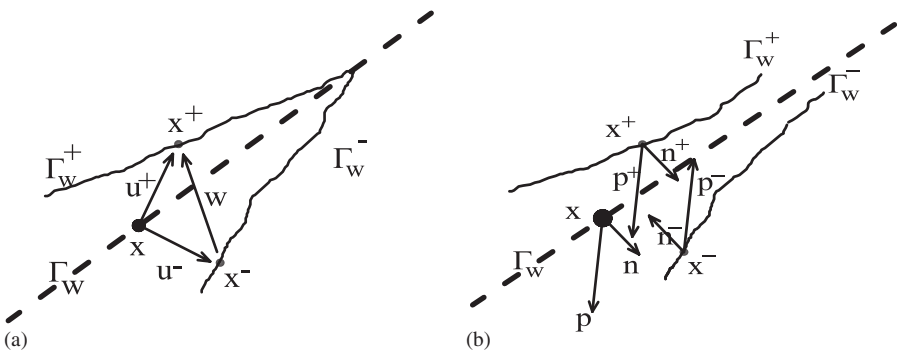

Figure 1. Description of the crack: Γ_w^+ and Γ_w^- represent 'deformed' crack lips as a subset of the deformed boundary: (a) geometry; and (b) static.

investigations are still an on going research point in view of the importance of LEFM in structural analysis at any length-scale.

In the present note, small strains and displacements hypothesis is assumed on a polygonal domain $\Omega \subset \mathbb{R}^2$, together with an isotropic linear elastic constitutive law in the homogeneous closed domain $\bar{\Omega}$. The structural response to the following quasi-static external actions is sought: tractions $\bar{\mathbf{p}}(\mathbf{x})$ on $\Gamma_p \subset \partial\Omega$, displacements $\bar{\mathbf{u}}(\mathbf{x})$ on $\Gamma_u \subset \partial\Omega$ and domain forces $\bar{\mathbf{f}}(\mathbf{x})$ in Ω.

A locus[‡] Γ_w of possible displacement discontinuities $\mathbf{w}(\mathbf{x})$ is allowed for and defined as follows: consider (see Figure 1) the two boundaries $\Gamma_w^+ \subset \partial\Omega$, $\Gamma_w^- \subset \partial\Omega$ modelling the lips of the crack, a reference surface Γ_w, and two one-to-one applications $\mathbf{u}^+ : \Gamma_w \to \Gamma_w^+$ and $\mathbf{u}^- : \Gamma_w \to \Gamma_w^-$ such that

$$\forall \mathbf{x}^+ \in \Gamma_w^+ \; \exists\, !\mathbf{x} \in \Gamma_w : \mathbf{u}^+ = \mathbf{x}^+ - \mathbf{x} \qquad \forall \mathbf{x}^- \in \Gamma_w^- \exists !\mathbf{x} \in \Gamma_w : \mathbf{u}^- = \mathbf{x}^- - \mathbf{x}$$

The function 'relative opening displacement' $\mathbf{w}(\mathbf{x}) : \Gamma_w \to \mathbb{R}^2$ is defined as follows:[§]

$$\mathbf{w}(\mathbf{x}) \stackrel{\text{def}}{=} \mathbf{u}^+ - \mathbf{u}^- \tag{1}$$

On both $\Gamma_w^+ \subset \partial\Omega$, $\Gamma_w^- \subset \partial\Omega$ outward normal—say $\mathbf{n}^+ \stackrel{\text{def}}{=} \mathbf{n}(\mathbf{x}^+)$, $\mathbf{n}^- \stackrel{\text{def}}{=} \mathbf{n}(\mathbf{x}^-)$—are defined by the path along the boundary itself (see Figure 1). The hypothesis of small displacements and strains implies $\mathbf{n}^+ = -\mathbf{n}^-$ and:

$$\int_{\Gamma_w^+} f(x)\, \mathrm{d}\Gamma_x = \int_{\Gamma_w^-} f(x)\, \mathrm{d}\Gamma_x = \int_{\Gamma_w} f(x)\, \mathrm{d}\Gamma_x$$

[‡]For the sake of clarity and in view of the goal of the paper it suffices to consider a unique crack, i.e. $\partial\Omega = \Gamma_p + \Gamma_u + \Gamma_w^+ + \Gamma_w^-$. The formulation in the presence of a generic number of cracks can be found, e.g. in [3].

[§]By definition (1) $\mathbf{w}$ may also model material interpenetration when $\mathbf{w} \cdot \mathbf{n} > 0$, with $\mathbf{n}$ defined by Equation (3). The problem of unilateral contact is not considered here, the reader is referred to a wide bibliography on the topic, see e.g. [4].

DOI: 10.1002/nme

$\forall f$ such that integrals take sense. Denoting with $\mathbf{p}(\mathbf{x}, \mathbf{n}(\mathbf{x}))$ the traction at point $\mathbf{x}$ across a surface of normal $\mathbf{n}(\mathbf{x})$ and with $\mathbf{p}^+ \stackrel{\text{def}}{=} \mathbf{p}(\mathbf{x}, \mathbf{n}^+)$, $\mathbf{p}^- \stackrel{\text{def}}{=} \mathbf{p}(\mathbf{x}, \mathbf{n}^-)$ the tractions on the two lips of the crack, the hypothesis of small displacements has the following implication on the local equilibrium conditions on $\Gamma_w^+ \cup \Gamma_w^-$:

$$\mathbf{p}^+ = -\mathbf{p}^- \tag{2}$$

Along Γ_w the outward normal can only be assumed by convention. In fact, Γ_w does not separate the body into two 'interior' and an 'external' parts, but it is a locus of 'displacement discontinuities'. A normal $\mathbf{n}(\mathbf{x})$ on Γ_w will be defined consistently with the definition of the relative opening displacement $\mathbf{w}$. The power due to tractions on $\Gamma_w^+ \cup \Gamma_w^-$,

$$\delta\dot{W} = \mathbf{p}^+ \cdot \dot{\mathbf{u}}^+ + \mathbf{p}^- \cdot \dot{\mathbf{u}}^- = \mathbf{p}^+ \cdot (\dot{\mathbf{u}}^+ - \dot{\mathbf{u}}^-) = \mathbf{p}^+ \cdot \dot{\mathbf{w}}$$

naturally lead to define:

$$\mathbf{p}(\mathbf{x}) \stackrel{\text{def}}{=} \mathbf{p}^+ \quad \mathbf{n}(\mathbf{x}) \stackrel{\text{def}}{=} \mathbf{n}^+ \quad \mathbf{x} \in \Gamma_w \tag{3}$$

Tractions $\mathbf{p}$ and relative opening displacements $\mathbf{w}$ may be related by a nonlinear vector function in case of cohesive traction problems [3]: in the present note though, $\mathbf{p}$ at $\mathbf{x} \in \Gamma_w$ is assumed to be a given term—eventually zero—denoted with $\bar{\mathbf{p}}_w$ to model pressurized cracks in the LEFM framework.

The boundary integral formulation of a LEFM problem stems from Somigliana's identity [5]:

$$\begin{aligned} &\mathbf{u}(\mathbf{x}) + \int_{\partial\Omega} \mathbf{G}_{up}(\mathbf{x} - \mathbf{y}; \mathbf{l}(\mathbf{y}))\mathbf{u}(\mathbf{y})\, d\mathbf{y} \\ &\quad = \int_{\partial\Omega} \mathbf{G}_{uu}(\mathbf{x} - \mathbf{y})\mathbf{p}(\mathbf{y})\, d\mathbf{y} + \int_{\Omega} \mathbf{G}_{uu}(\mathbf{x} - \mathbf{y})\bar{\mathbf{f}}(\mathbf{y})\, d\mathbf{y}, \quad \mathbf{x} \in \Omega \end{aligned} \tag{4}$$

which is the boundary integral representation (BIR) of displacements in the interior of the domain. Somigliana's identity is based on Green's functions (also called kernels—see [6, Appendix A]) which represent components u_i of the displacement vector $\mathbf{u}$ in a point $\mathbf{x}$ due to: (i) a unit force concentrated in space (point $\mathbf{y}$) and acting on the unbounded elastic space Ω_∞ in direction j (such functions are gathered in matrix $\mathbf{G}_{uu}(\mathbf{x}-\mathbf{y})$); (ii) a unit relative displacement concentrated in space (at a point $\mathbf{y}$), crossing a surface with normal $\mathbf{l}(\mathbf{y})$ and acting on the unbounded elastic space Ω_∞ (in direction j) (gathered in matrix $\mathbf{G}_{up}(\mathbf{x} - \mathbf{y})$). In view of the small displacement hypothesis, it holds:

$$\begin{aligned} &\int_{\Gamma_w^+ \cup \Gamma_w^-} \mathbf{G}_{up}(\mathbf{x} - \mathbf{y}; \mathbf{l}(\mathbf{y}))\mathbf{u}(\mathbf{y})\, d\mathbf{y} = \int_{\Gamma_w} \mathbf{G}_{up}(\mathbf{x} - \mathbf{y}; \mathbf{l}(\mathbf{y}))\mathbf{w}(\mathbf{y})\, d\mathbf{y} \\ &\int_{\Gamma_w^+ \cup \Gamma_w^-} \mathbf{G}_{uu}(\mathbf{x} - \mathbf{y})\mathbf{p}(\mathbf{y})\, d\mathbf{y} = \mathbf{0} \end{aligned} \tag{5}$$

It worths to stress that identity (5) represents a mathematical degeneracy, whose consequence is 'the loss of existence and uniqueness of the solution. It is clear that there exists in the theory of elasticity a fundamental problem of a lack of a general integral formulation for problems of an elastic body with degenerate geometry that encloses no area or volume. A single integral equation

DOI: 10.1002/nme

of elasticity derived from Somigliana's identity is too slim to solve general elastic crack problems.' (taken from [7]).

To obtain an additional integral equation, the traction operator can be applied to Somigliana's identity,[¶] thus obtaining the BIR of tractions on a surface of normal $\mathbf{n}(\mathbf{x})$ in the interior of the domain [8]:

$$\begin{aligned}\mathbf{p}(\mathbf{x},\mathbf{n}(\mathbf{x})) &+ \int_{\Gamma_p} \mathbf{G}_{pp}(\mathbf{r};\mathbf{n}(\mathbf{x});\mathbf{l}(\mathbf{y}))\mathbf{u}(\mathbf{y})\,d\mathbf{y} + \int_{\Gamma_u} \mathbf{G}_{pp}(\mathbf{r};\mathbf{n}(\mathbf{x});\mathbf{l}(\mathbf{y}))\bar{\mathbf{u}}(\mathbf{y})\,d\mathbf{y} \\ &+ \int_{\Gamma_w} \mathbf{G}_{pp}(\mathbf{r};\mathbf{n}(\mathbf{x});\mathbf{l}(\mathbf{y}))\mathbf{w}(\mathbf{y})\,d\mathbf{y} \\ &= \int_{\Gamma_u} \mathbf{G}_{pu}(\mathbf{r};\mathbf{n}(\mathbf{x}))\mathbf{p}(\mathbf{y})\,d\mathbf{y} + \int_{\Gamma_p} \mathbf{G}_{pu}(\mathbf{r};\mathbf{n}(\mathbf{x}))\bar{\mathbf{p}}(\mathbf{y})\,d\mathbf{y} \\ &+ \int_{\Omega} \mathbf{G}_{pu}(\mathbf{r};\mathbf{n}(\mathbf{x}))\bar{\mathbf{f}}(\mathbf{y})\,d\mathbf{y}, \quad \mathbf{x}\in\Omega \end{aligned} \tag{6}$$

having denoted with $\mathbf{r}=\mathbf{x}-\mathbf{y}$. Such a BIR involves Green's functions (collected in matrices $\mathbf{G}_{pu}$ and $\mathbf{G}_{pp}$[‖]) which describe components (p_i) of the traction vector $\mathbf{p}$ on a surface of normal $\mathbf{n}(\mathbf{x})$ due to: (i) a unit force concentrated in space (point $\mathbf{y}$) and acting on the unbounded elastic space Ω_∞ in direction j; (ii) a unit relative displacement concentrated in space (at a point $\mathbf{y}$), crossing a surface with normal $\mathbf{l}(\mathbf{y})$ and acting on the unbounded elastic space Ω_∞ (in direction j).

BIEs for the linear elastic problem can be derived from BIRs (4) and (6) by performing the boundary limit[**] $\Omega \ni \mathbf{x} \to \mathbf{x}^o \in \Gamma$. In the limit process, extensively investigated[††] singularities of Green's functions are triggered off: their singularity-orders are collected in Table I.

Strongly singular kernels $\mathbf{G}_{up}$ and $\mathbf{G}_{pu}$ generate free terms in the limit process, $\mathbf{C}(\mathbf{x})$ and $\mathbf{D}(\mathbf{x})$ respectively, that holds $\frac{1}{2}\mathbf{I}$ for smooth boundaries [10, 15, 16]. It has been shown [17, 18] that also the hypersingular kernel generates a free term when there is a curvature discontinuity and/or a discontinuity of the tangent vector to the boundary at a point where at least one adjacent boundary

[¶] The above introduced kernels are infinitely smooth in their domain, which is the whole space $\mathbb{R}^2$ with exception of the origin (that is $\mathbf{x}\neq\mathbf{y}$).

[‖] Kernel $\mathbf{G}_{pp}$ is usually named hypersingular, since it shows a singularity greater than the dimension of the integral [9].

[**] For (6) the boundary limit must be taken at a smooth point $\mathbf{x}^o$ with a well-defined normal vector $\mathbf{n}(\mathbf{x}^o)$ [10].

[††] By the approach of [11], all singular terms cancel out in the limit process (and without recourse to any *a priori* interpretation in the finite part sense). However, there exists an intimate relationship between hypersingular BIEs and finite part integrals (HFP) in the sense of Hadamard [12]. In [9, 13] among others, it has been proved that a hypersingular integral can be interpreted as a HFP in the limit as an internal point source approaches the boundary. In [14], the same conclusion has been obtained by an alternate definition of HFP, without the need for a limiting process. Making recourse to the distribution theory, in [7] the dual BIEs are obtained by the application of a trace operator to the representation formulae. In such an approach, the strongly singular and hypersingular integrals can be expressed by means of discontinuity jumps (also named 'free terms') of these integrals on the boundary summed with the values of the integrals on the boundary existing only in the sense of Cauchy principal value (CPV) or in the sense of the HFP. By exploiting Green's functions properties, the commutativity of the two operations of traction and trace has also been proved, showing the consistency of all different approaches of derivations of the BIEs.

DOI: 10.1002/nme

Table I. Kernels and their singularities. Here $\mathbf{r} \stackrel{\text{def}}{=} \mathbf{x} - \mathbf{y}$ and $r = \|\mathbf{r}\|$.

	Asymptotical behaviour when $\mathbf{r} \to \mathbf{0}$			Relevant 'integrals' when $\mathbf{x} \in \partial\Omega$	
Kernel	2D	3D	Denomination of singularity	Nature	Symbol
$\mathbf{G}_{uu}$	$O(\log(r))$	$O(r^{-1})$	Weak (integrable)	Lebesgue	$\int$
$\mathbf{G}_{up}$,$\mathbf{G}_{pu}$	$O(r^{-1})$	$O(r^{-2})$	Strong	CPV	$⨍$
$\mathbf{G}_{pp}$	$O(r^{-2})$	$O(r^{-3})$	Hyper	HFP	$⨎$

part is curved. Assuming smooth boundaries, the following BIEs come out:

$$\frac{1}{2}\mathbf{u}(\mathbf{x}) + \int_{\Gamma_p} \mathbf{G}_{up}(\mathbf{r};\mathbf{l}(\mathbf{y}))\mathbf{u}(\mathbf{y})\,\mathrm{d}\,\mathrm{d}\mathbf{y} + \int_{\Gamma_u} \mathbf{G}_{up}(\mathbf{r};\mathbf{l}(\mathbf{y}))\bar{\mathbf{u}}(\mathbf{y})\,\mathrm{d}\mathbf{y} + \int_{\Gamma_w} \mathbf{G}_{up}(\mathbf{r};\mathbf{l}(\mathbf{y}))\mathbf{w}(\mathbf{y})\,\mathrm{d}\mathbf{y}$$
$$= \int_{\Gamma_u} \mathbf{G}_{uu}(\mathbf{r})\mathbf{p}(\mathbf{y})\,\mathrm{d}\mathbf{y} + \int_{\Gamma_p} \mathbf{G}_{uu}(\mathbf{r})\bar{\mathbf{p}}(\mathbf{y})\,\mathrm{d}\mathbf{y} + \int_{\Omega} \mathbf{G}_{uu}(\mathbf{r})\bar{\mathbf{f}}(\mathbf{y})\,\mathrm{d}\mathbf{y}, \quad \mathbf{x} \in \partial\Omega \tag{7}$$

$$\frac{1}{2}\mathbf{p}(\mathbf{x}) + ⨍_{\Gamma_p} \mathbf{G}_{pp}(\mathbf{r};\mathbf{n}(\mathbf{x});\mathbf{l}(\mathbf{y}))\mathbf{u}(\mathbf{y})\,\mathrm{d}\mathbf{y} + ⨍_{\Gamma_u} \mathbf{G}_{pp}(\mathbf{r};\mathbf{n}(\mathbf{x});\mathbf{l}(\mathbf{y}))\bar{\mathbf{u}}(\mathbf{y})\,\mathrm{d}\mathbf{y}$$
$$+ ⨍_{\Gamma_w} \mathbf{G}_{pp}(\mathbf{r};\mathbf{n}(\mathbf{x});\mathbf{l}(\mathbf{y}))\mathbf{w}(\mathbf{y})\,\mathrm{d}\mathbf{y}$$
$$= ⨍_{\Gamma_u} \mathbf{G}_{pu}(\mathbf{r};\mathbf{n}(\mathbf{x}))\mathbf{p}(\mathbf{y})\,\mathrm{d}\mathbf{y} + ⨍_{\Gamma_p} \mathbf{G}_{pu}(\mathbf{r};\mathbf{n}(\mathbf{x}))\bar{\mathbf{p}}(\mathbf{y})\,\mathrm{d}\mathbf{y}$$
$$+ ⨍_{\Omega} \mathbf{G}_{pu}(\mathbf{r};\mathbf{n}(\mathbf{x}))\bar{\mathbf{f}}(\mathbf{y})\,\mathrm{d}\mathbf{y}, \quad \mathbf{x} \in \partial\Omega \tag{8}$$

Equation (7) is referred to as 'displacement equation', whereas Equation (8) is named 'traction equation'. After imposing the fulfillment of Equation (7) on the Dirichlet boundary Γ_u and of equation (8) on the Neumann boundary Γ_p as well as on the conventional boundary Γ_w, the following linear boundary integral problem comes out:

$$\begin{bmatrix} \int_{\Gamma_u} \mathbf{G}_{uu}[.]\mathrm{d}\mathbf{y} & -⨍_{\Gamma_p} \mathbf{G}_{up}[.]\,\mathrm{d}\mathbf{y} & -⨍_{\Gamma_w} \mathbf{G}_{up}[.]\,\mathrm{d}\mathbf{y} \\ -⨍_{\Gamma_u} \mathbf{G}_{pu}[.]\,\mathrm{d}\mathbf{y} & ⨎_{\Gamma_p} \mathbf{G}_{pp}[.]\,\mathrm{d}\mathbf{y} & ⨎_{\Gamma_w} \mathbf{G}_{pp}[.]\,\mathrm{d}\mathbf{y} \\ -⨍_{\Gamma_u} \mathbf{G}_{pu}[.]\,\mathrm{d}\mathbf{y} & ⨎_{\Gamma_p} \mathbf{G}_{pp}[.]\,\mathrm{d}\mathbf{y} & ⨎_{\Gamma_w} \mathbf{G}_{pp}[.]\,\mathrm{d}\mathbf{y} \end{bmatrix} \begin{bmatrix} \mathbf{p} \\ \mathbf{u} \\ \mathbf{w} \end{bmatrix} = \begin{bmatrix} \mathbf{f}^u \\ \mathbf{f}^p \\ \mathbf{f}^w \end{bmatrix} \begin{matrix} \mathbf{x} \in \Gamma_u \\ \mathbf{x} \in \Gamma_p \\ \mathbf{x} \in \Gamma_w \end{matrix} \tag{9}$$

DOI: 10.1002/nme

Vectors $\mathbf{f}^i$, $i = u, p, w$, that gather all data (i.e. $\bar{\mathbf{p}}$, $\bar{\mathbf{p}}_w$, $\bar{\mathbf{u}}$, $\bar{\mathbf{f}}$) follows:

$$\mathbf{f}^u(\mathbf{x}) := \frac{1}{2}\bar{\mathbf{u}} - \int_{\Gamma_p} \mathbf{G}_{uu}\bar{\mathbf{p}}\,\mathrm{d}\mathbf{y} + \oint_{\Gamma_u} \mathbf{G}_{up}\bar{\mathbf{u}}\,\mathrm{d}\mathbf{y} - \int_{\Omega} \mathbf{G}_{uu}\bar{\mathbf{f}}\,\mathrm{d}\mathbf{y}$$

$$\mathbf{f}^p(\mathbf{x}) := -\frac{1}{2}\bar{\mathbf{p}} + \oint_{\Gamma_p} \mathbf{G}_{pu}\bar{\mathbf{p}}\,\mathrm{d}\mathbf{y} - \oint_{\Gamma_u} \mathbf{G}_{pp}\bar{\mathbf{u}}\,\mathrm{d}\mathbf{y} + \int_{\Omega} \mathbf{G}_{pu}\bar{\mathbf{f}}\,\mathrm{d}\mathbf{y}$$

$$\mathbf{f}^w(\mathbf{x}) := -\bar{\mathbf{p}}_w + \oint_{\Gamma_p} \mathbf{G}_{pu}\bar{\mathbf{p}}\,\mathrm{d}\mathbf{y} - \oint_{\Gamma_u} \mathbf{G}_{pp}\bar{\mathbf{u}}\,\mathrm{d}\mathbf{y} + \int_{\Omega} \mathbf{G}_{pu}\bar{\mathbf{f}}\,\mathrm{d}\mathbf{y}$$

Integral problem (9) can be written in the compact form:

$$\mathscr{L}[y] = f \tag{10}$$

with all terms defined by comparison. Unknown vector y is made of tractions $\mathbf{p}$ on the Dirichlet boundary Γ_u, displacements $\mathbf{u}$ on the Neumann boundary Γ_p, relative opening displacements $\mathbf{w}$ along the crack Γ_w. Denote with $Y_{\mathscr{L}}$ the domain of $\mathscr{L}$ and with $F_{\mathscr{L}}$ its range. Let bilinear form $\mathscr{A}_{\mathscr{L}} : Y_{\mathscr{L}} \times Y_{\mathscr{L}} \to \mathbb{R}$:

$$\mathscr{A}_{\mathscr{L}}(a, b) \stackrel{\text{def}}{=} \int_{\partial\Omega} \mathscr{L}[\,a(\mathbf{y})](\mathbf{x}) b(\mathbf{x})\,\mathrm{d}\Gamma(\mathbf{x}) \tag{11}$$

It can be proved—starting from the property of reciprocity [8]—that bilinear form $\mathscr{A}_{\mathscr{L}}$ is symmetric:

$$\mathscr{A}_{\mathscr{L}}(a, b) = \mathscr{A}_{\mathscr{L}}(b, a) \quad \forall a, b \in Y_{\mathscr{L}}$$

As a consequence, the solution of problem (10) is a critical point of functional

$$\Psi[y] = \frac{1}{2}\mathscr{A}_{\mathscr{L}}(y, y) - \int_{\partial\Omega} y(\mathbf{x}) f(\mathbf{x})\,\mathrm{d}\Gamma(\mathbf{x})$$

extensively written in [19].

Let $h > 0$ be a parameter and let $[\mathbf{p}_h(\mathbf{y}), \mathbf{u}_h(\mathbf{y}), \mathbf{w}_h(\mathbf{y})]^{\mathsf{T}} \stackrel{\text{def}}{=} y_h \in Y_{\mathscr{L}h}$ be an approximation of the unknown vector field y, denoting with $Y_{\mathscr{L}h}$ a family of finite dimensional subspaces of $Y_{\mathscr{L}}$ such that

$$\forall y \in Y_{\mathscr{L}}, \inf_{y_h \in Y_{\mathscr{L}h}} \|y - y_h\| \to 0 \quad \text{as } h \to 0 \tag{12}$$

Discretization (12) allows to transform integral problem (10) into a set of algebraic equations. Two main techniques have been successfully developed to this aim: the collocation boundary element method (CBEM) [5] and the symmetric Galerkin [20] method (SGBEM).

In the case of $\Gamma_w = \emptyset$, displacement equation (7) is the starting point for the numerical approximation via the CBEM. In modelling fracture mechanics problems with $\Gamma_w \neq \emptyset$, identity (5) represents an insurmountable mathematical difficulty in applying the CBEM making use of the displacement equation only (see e.g. [21, 22]). Several special techniques have been devised to overcome this mathematical degeneracy: among others, the special Green's functions methods

DOI: 10.1002/nme

[23], the zone method [24] and the Dual BEM [25]. Starting from problem (10) CBEM requires the fulfillment of integral equations

$$\mathscr{L}[y_h] = f$$

onto a selected set of collocation points $\mathbf{x}_i^* \in \partial\Omega$. In this technique 'integrals' of the form:

$$\int_{\Gamma_s} \mathbf{G}_{rs}(\mathbf{x}_i^* - \mathbf{y})\psi_h(\mathbf{y}) : \mathrm{d}\Gamma(\mathbf{y}) \quad r = u, \quad s = u, p \tag{13}$$

must be tackled, denoting with $\psi_h(\mathbf{y})$ *scalar* shape functions for modelling the components of approximation y_h of the unknown vector fields along $\partial\Omega$.

The SGBEM approximation of (10) consists in finding $y_h \in Y_{\mathscr{L}h}$ critical point of the functional:

$$\Psi[y_h] = \frac{1}{2}\mathscr{A}_{\mathscr{L}}(y_h, y_h) - \int_{\partial\Omega} y_h(\mathbf{x}) f(\mathbf{x})\, \mathrm{d}\Gamma(\mathbf{x})$$

By imposing the stationarity of $\Psi[y_h]$ with respect to the set of nodal values, one deals with integrals of the following form:

$$\int_{\Gamma_r} \psi_k(\mathbf{x}) \int_{\Gamma_s} \mathbf{G}_{rs}(\mathbf{x}, \mathbf{y})\psi_h(\mathbf{y})\, \mathrm{d}\Gamma(\mathbf{y})\, \mathrm{d}\Gamma(\mathbf{x}), \quad r, s = u, p \tag{14}$$

where $\psi_k(\mathbf{x})$, $\psi_h(\mathbf{y})$ are *scalar* test and shape functions that model the components of the unknown vector fields along the boundary.

In the numerical approximation of LEFM problems, a correct representation of the local stress and displacement fields in the neighbourhood of the crack tip is essential for accurate evaluation of SIFs: as they govern initiation, propagation and stability of fractures [26], their determination is of primary importance. As well known, displacement field $\mathbf{u}(\mathbf{x})$ around the crack tip asymptotically behaves as $\sqrt{\rho}$, denoting with $\rho = \|\mathbf{x} - \mathbf{x}_{Tip}\|$; consequently, the stress field $\boldsymbol{\sigma}(\mathbf{x})$ shows an asymptotic $\sqrt{\rho^{-1}}$ singularity at the crack tip [27]. Incorporating the asymptotic behaviour $\sqrt{\rho}$ in shape functions $\psi_k(\mathbf{x})$, $\psi_h(\mathbf{y})$, by means of the 'quarter point element' [28, 29], significantly improved the accuracy of SIFs evaluation: nevertheless, poor precision resulted in SIFs approximation for several mixed-mode problems. A further improvement of quarter point elements was proposed in [30], insuring that the interpolated crack opening displacement $\mathbf{w}(\mathbf{x})$ satisfied a known constraint, the asymptotic vanishing of the term that is linear in distance to the crack tip. A 'modified quarter point element' (shortened in MQP), including a $\rho^{3/2}$ contribution, has been implemented in [31] and its evolution (named 'enhanced quarter point element') is proposed in Section 3. It concerns a higher order special crack tip element, based on a set of cubic lagrangian shape functions, with internal nodes suitably 'moved' in order to reproduce the desired asymptotic behaviour $\sqrt{\rho}$ in shape functions $\psi_k(\mathbf{x})$, $\psi_h(\mathbf{y})$; the asymptotic vanishing of the term that is linear in distance to the crack tip is also enforced. It is expected, and indeed shown in all numerical examples in Section 7, that using higher order elements will increase the accuracy of SIFs approximation with respect to the MQP in the spirit of the usual p-refinement.

The evaluation of (13)–(14) is never a trivial task, because of the involved singularities, especially for the hypersingular kernel. Several techniques, collectable in three principal groups, have been proposed for their evaluation: (i) regularization techniques, (ii) numerical integrations, (iii) analytical integrations. By a *regularization procedure*, the strongly singular and hypersingular integrals are analytically manipulated to convert them into, at most, weakly singular integrals,

DOI: 10.1002/nme

which can then be computed throughout different quadrature schemes. Regularization procedures have been obtained by means of simple solutions [32, 33]; by applying the Stokes theorem [13, 34]; via integration by parts [35]. *Numerical methods* for the evaluation of the CPV were proposed first in [36]. There is nowadays an extensive literature on this subject (see, among others [37]). A huge amount of literature concerns the numerical evaluation of hypersingular integrals: among others, see [38, 39]. *Analytical integrations* have been basically performed towards three schemes. In the first scheme (see e.g. [11, 40]), the source point is fixed, while the boundary around the source point is temporarily deformed to allow an analytical evaluation of contributions from singular kernels, and then the limit is taken as the deformed boundary shrinks back to the actual boundary. In a second approach, see among others [41–43], the source point $\mathbf{x}$ is first moved away from the boundary; integrals are evaluated analytically and a limit process is then performed to bring the source point back to the boundary. In all the aforementioned papers, analytical integrations are provided for all singular integrals, while standard quadrature formulae are used for non-singular integrals. In the third scheme [6, 44], the complete analytical integration has been provided, directly evaluating HFP and CPV as well as by means of a limit to the boundary process.

The present note aims at extending analytical integrations proposed in [6] to LEFM. It focuses on the closed form of the single integration process (13) pertaining to the CBEM, in Section 4, and proves, in Section 5.1, the integrability of (13) in a Lebesgue sense required by SGBEM in Equation (14). Discretization is considered by means of straight elements adopting polynomial test and shape functions of arbitrary degree away of the crack tip, and higher-order modified quarter point shape functions, detailed in section 3, in the vicinity of the crack tip. All possible singularities described in Table I are taken into account in Section 4, performing a direct evaluation of CPV and HFP as well as a limit to the boundary $\mathbf{x} \to \partial\Omega$ of analytical integrations at $\mathbf{x} \in \Omega$.

The proposed closed form of integral (13): (i) takes advantage of the definition of two maps, named ϑ and h, analysed in Sections 2.1 and 2.2, respectively; (ii) exploits and algebraic manipulates basic integrals that for the sake of readability are collected in Appendix B; (iii) is the linear combination of a few basic functions, that are the essence of the asymptotical behaviour of the solution, by means of suitable matrices collected in Appendix C; (iv) permits, comparing Westergaard's asymptotic analysis [45] with the asymptotic analysis of traction BIR (6), the formulation in Section 6 of a displacement correlation formula for the approximation of SIFs which is coherent with the approximated stress field around the crack tip.

It seems to be worth noting that such a displacement correlation formula can also be derived from the 'two-point' formula approach which though has a different nature, coming out from William's asymptotic analysis of the displacement field near the crack tip apart of any discretization process. Such an equivalence seem to reveal that the two-point formula is privileged in the framework of LEFM via BIEs with respect to all other SIFs approximation formulas, which are based on indirect measures of SIFs but do not match the limit to the crack tip of the approximated stress field. The interest in analytical integrations therefore is not limited to computational efficiency; nevertheless, 'measuring' the computational cost of their implementation can be of interest and has been performed in Section 4.5.

An object-oriented computer code, that implements the proposed integration schemes, has been developed and is available for the scientific community. By means of it, numerical analysis for SIFs approximation have been performed over a set of academical examples and benchmarks in Section 7. Further publications will be devoted to more extensive analysis of real-life engineering problems.

DOI: 10.1002/nme

2. TWO MAPPINGS

Analytical integrations of (13) and (14) that will be performed in Section 4 make use of two mappings $\vartheta : \mathbb{R}^2 \times \mathbb{R}_0^+ \to \mathbb{R}$ and $h : \mathbb{R}^2 \times \mathbb{R}_0^+ \to \mathbb{R}$ that, because of their complexity, worth to be detailed in a separate section.

2.1. Mapping $\vartheta(\mathbf{d}; \alpha)$

Consider interval $\mathscr{I}_\xi = [-l, l]$, a local co-ordinate system $\{0, \boldsymbol{\xi}\}$ and assume the crack tip at $\xi_1 = l$ as in Figure 2. Let $\mathbf{d}$ be the position vector after a reference change $d_1 = l - \xi_1, d_2 = -\xi_2$ from $\{0, \boldsymbol{\xi}\}$ to $\{\text{Tip}, \mathbf{d}\}$ as in Figure 2. Consider a parameter $\alpha \in \mathbb{R}_0^+$ and mapping $\vartheta_\kappa : \mathbb{R}^2 \times \mathbb{R}_0^+ \to \mathbb{R}$ defined when $d_2 \neq 0$ by

$$\vartheta_\kappa(\mathbf{d}; \alpha) = \begin{cases} \arctan\left[\dfrac{\sqrt{2}|\mathbf{d}| - (-1)^\kappa \alpha \sqrt{|\mathbf{d}| + d_1}}{\alpha \sqrt{|\mathbf{d}| - d_1}}\right] \operatorname{sgn}(d_2) & \text{if } \alpha \neq 0 \\ \dfrac{\pi}{2} \operatorname{sgn}(d_2) & \text{if } \alpha = 0 \end{cases} \tag{15}$$

with[‡‡] $\kappa \in \{0, 1\}$ and $|\mathbf{d}| = \sqrt{d_1^2 + d_2^2}$. The following properties hold:

$$\vartheta_\kappa(\mathbf{d}; \alpha) = -\frac{\sqrt{|\mathbf{d}| - d_1}}{\sqrt{2}} \operatorname{sgn}(d_2) \int \frac{1}{\alpha^2 - (-1)^\kappa \sqrt{2} \alpha \sqrt{|\mathbf{d}| + d_1} + |\mathbf{d}|} \, \mathrm{d}\alpha \tag{16}$$

$$\vartheta(\{d_1, -d_2\}; \alpha) = -\vartheta(\{d_1, d_2\}; \alpha) \tag{17}$$

Integral (16) is well-defined $\forall \alpha$ when[§§] $|\mathbf{d}| \neq 0$. In view of property (17), only the behaviour of ϑ_κ in half-plane $d_2 > 0$ will be studied.

For being $\alpha \in \mathbb{R}_0^+$, the behaviour of mapping ϑ_1 in a neighbourhood of $|\mathbf{d}| = d_1 \neq 0$ obeys the following proposition:

$$\lim_{d_2 \to 0^+} \vartheta_1(\mathbf{d}; \alpha)\Big|_{d_1 > 0} = \frac{\pi}{2} \quad \forall \alpha \tag{18}$$

To study mapping ϑ_0 onto half-line $d_2 = 0, d_1 > 0$, two separate regions must be taken into account:[¶¶]

$$\lim_{d_2 \to 0^+} \vartheta_0(\mathbf{d}; \alpha)\Big|_{d_1 > 0} = \begin{cases} \dfrac{\pi}{2} & \text{if } [\alpha \neq 0 \text{ and } d_1 > \alpha^2] \text{ or } [\alpha = 0] \\ -\dfrac{\pi}{2} & \text{if } [\alpha \neq 0 \text{ and } 0 < d_1 < \alpha^2] \end{cases} \tag{19}$$

[‡‡] Mapping ϑ_κ, whose geometrical interpretation is an angle hard to be depicted, comes into play in analytical integrations when $\alpha = \sqrt{2l}$ and $\alpha = 0$ (see Figure 2).

[§§] I.e. when $\boldsymbol{\xi}$ differs from the crack tip.

[¶¶] If one would extend mapping $\vartheta_0(\mathbf{d}; \alpha)$ accordingly to Equation (19) to half-line $d_2 = 0$, $d_1 > 0$, a discontinuity with respect to $\mathbf{d}$-easily seen in Figure 3—would appear at $d_1 = \alpha^2, d_2 = 0$.

DOI: 10.1002/nme

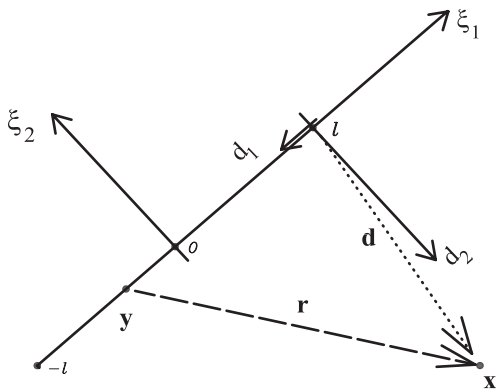

Figure 2. Local co-ordinate systems $\{0, \boldsymbol{\xi}\}$ and {Tip, $\mathbf{d}$}.

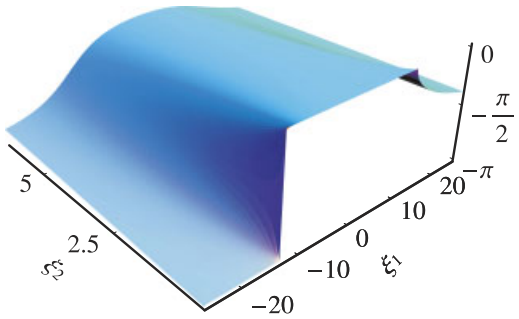

Figure 3. A plot of mapping $\vartheta(\mathbf{d}; \alpha)$ for $l = 13$, $-l < d_1 < 3l$, $-\frac{l}{2} < d_2 < 0$ and $\alpha = \sqrt{2l}$.

It is straightforward proving that on half-line $d_2 = 0$, $d_1 < 0$:

$$\lim_{d_2 \to 0^+} \vartheta_\kappa(\mathbf{d}; \alpha)\Big|_{d_1<0} = \begin{cases} \arctan \dfrac{\sqrt{|\mathbf{d}|}}{\alpha} & \text{if } \alpha \neq 0 \\ \dfrac{\pi}{2} & \text{if } \alpha = 0 \end{cases} \tag{20}$$

Define mapping $\vartheta : \mathbb{R}^2 \times \mathbb{R}_0^+ \to \mathbb{R}$ for $d_2 \neq 0$ as the sum of the two mappings:

$$\vartheta(\mathbf{d}; \alpha) = \vartheta_0(\mathbf{d}; \alpha) + \vartheta_1(\mathbf{d}; \alpha) \tag{21}$$

From Equations (17)–(19) mapping ϑ can be smoothly extended along the segment $0 < d_1 < \alpha^2$, $d_2 = 0$ by defining:

$$\vartheta(\{0 < d_1 < \alpha^2, 0\}; \alpha) = 0 \tag{22}$$

Mapping $\vartheta(\mathbf{d}; \alpha)$—which is bounded over any subset of $\mathbb{R}^2 \times \mathbb{R}_0^+$—is plotted in Figure 3 exploiting property (17).

DOI: 10.1002/nme

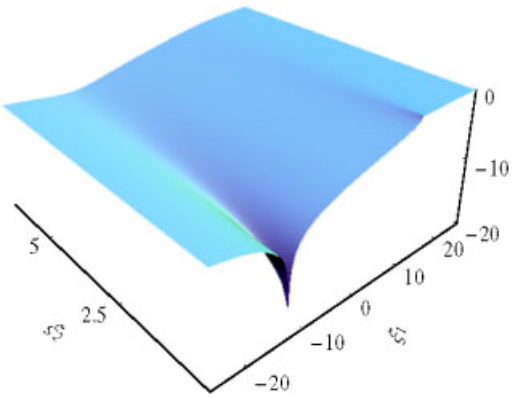

Figure 4. A plot of mapping $h(\mathbf{d};\alpha)$ for $l=13$, $-l<d_1<3l$, $0<d_2<\frac{l}{2}$ and $\alpha=\sqrt{2l}$.

2.2. *Mapping* $h(\mathbf{d};\alpha)$

Consider a parameter $\alpha\in\mathbb{R}_0^+$ and mapping $h_\kappa:\mathbb{R}^2\times\mathbb{R}_0^+\to\mathbb{R}$ defined by

$$h_\kappa(\mathbf{d};\alpha)=\log[\alpha^2-(-1)^\kappa\sqrt{2}\alpha\sqrt{|\mathbf{d}|+d_1}+|\mathbf{d}|] \tag{23}$$

with $\kappa\in\{0,1\}$. Mapping h_1 is defined in the whole set $\mathbb{R}^2\times\mathbb{R}_0^+$ with exception of its null point $\alpha=|\mathbf{d}|=0$. Mapping h_0 is not defined in the set

$$\mathbb{R}^2\times\mathbb{R}_0^+\supseteq\mathbf{Q}\stackrel{\text{def}}{=}\left\{\mathbf{d},\alpha|0\leqslant\alpha-\sqrt{2d_1-\alpha^2}\leqslant\sqrt{2}\sqrt{|\mathbf{d}|+d_1}\leqslant\alpha+\sqrt{2d_1-\alpha^2}\right\} \tag{24}$$

which reduces at point $d_1=2l$, $d_2=0$ for $\alpha=\sqrt{2l}$ and at the origin $|\mathbf{d}|=0$ for $\alpha=0$ (see Figure 2).

Define mapping $h:\mathbb{R}^2\times\mathbb{R}_0^+\to\mathbb{R}$ as the sum:

$$h(\mathbf{d};\alpha)=h_1(\mathbf{d};\alpha)-h_0(\mathbf{d};\alpha)=\log\frac{\alpha^2+\sqrt{2}\alpha\sqrt{|\mathbf{d}|+d_1}+|\mathbf{d}|}{\alpha^2-\sqrt{2}\alpha\sqrt{|\mathbf{d}|+d_1}+|\mathbf{d}|} \tag{25}$$

Mapping h inherits the non-definiteness in set $\mathbf{Q}$, but can be C^0-extended at $\alpha=|\mathbf{d}|=0$ by defining

$$h(\mathbf{0};0)=0 \tag{26}$$

Mapping $h(\mathbf{d};\alpha)$ is plotted in Figure 4 exploiting property $h(\{d_1,-d_2\};\alpha)=h(\{d_1,d_2\};\alpha)$.

3. ENHANCED QUARTER POINT SHAPE FUNCTIONS

Define test $\psi_k(\mathbf{x})$ and shape functions $\psi_h(\mathbf{y})$ in Equations (13)–(14) as follows. Let Γ_h be a decomposition of polygonal boundary Γ with nodes $\{P_h, h=1,2,\ldots,N_h\}$. Denote with T_j the generic segment[|||] of Γ_h that does not contain a crack tip and with l its half length; denote with T_{tip} the generic segment of Γ_h enclosing a crack tip and with l its half length. Assume a local

[|||] Segment or panel will be used as synonymous.

DOI: 10.1002/nme

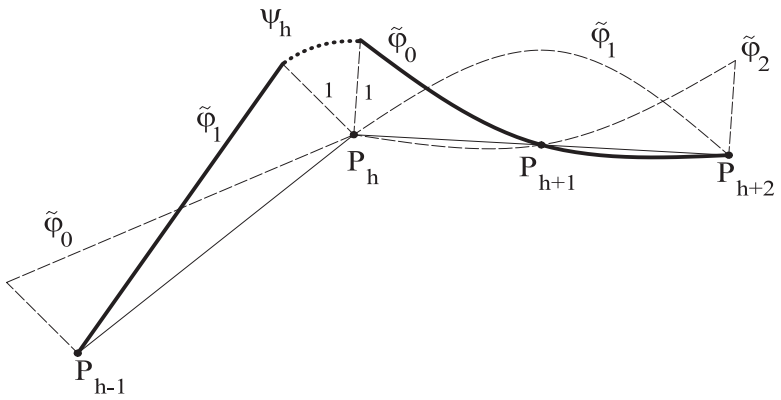

Figure 5. Local $\tilde{\varphi}_n(\xi_1(P))$ and global $\psi_h(\mathbf{y})$ shape functions.

co-ordinate system $\{0, \boldsymbol{\xi}\}$ over any panel*** T, such that $\xi_2(P)=0$ and $\xi_1(P)\in\mathscr{I}_\xi=[-l, l]$ for all $P\in T$, as in Figure 2. Assume that the crack tip is located at $\xi_1=l$ and select over T_{tip} a local basis $\{\tilde{\varphi}_0, \tilde{\varphi}_1, \tilde{\varphi}_2\}$, which will be extensively written at the end of the present section, by Equation (35). Choose over T_j a local basis $\{\tilde{\varphi}_0, \tilde{\varphi}_1, \ldots, \tilde{\varphi}_{N_j}\}$ where $\tilde{\varphi}_j$ denotes a polynomial (usually Lagrangian) of degree N_j defined on a subset of $\{P_h\}$ of N_j+1 nodes in T_j. Collect in set $\mathscr{T}_h$ the (two at most) panels sharing vertex P_h (see Figure 5); then ψ_h is defined as:

$$\psi_h(\mathbf{y}(P)) := \begin{cases} \tilde{\varphi}_n(\xi_1(P)) & \text{if } T\in\mathscr{T}_h \\ 0 & \text{if } T\notin\mathscr{T}_h \end{cases} \qquad P\in T \tag{27}$$

where index $0\leqslant n\leqslant \max\{2, N_j\}$ selects the unique local basis function on T such that $\tilde{\varphi}_n(\xi_1(P_h))=1$. By construction, $\psi_h(\mathbf{y})$ is continuous over Γ_h, and its support coincides with $\mathscr{T}_h$.

Consider the uniform partition $\mathscr{P}$ of interval $\mathscr{I}_s \overset{\text{def}}{=} [-1, 1]$ defined by means of points $P_i=-1+\frac{2i}{3}$ with $i=0, 1, 2, 3$. Assume over $\mathscr{P}$ as shape function basis $\boldsymbol{\Upsilon} \overset{\text{def}}{=} \{\zeta_j, j=0, 1, 2, 3\}$ with the four lagrangian cubic polynomials $\zeta_j(s)$, such that $s\in\mathscr{I}_s$ and $\zeta_j(P_i)=\delta_{ij}$. In the spirit of [28] and of [29], define the crack tip (at $\xi=l$) geometry by means of mapping $\xi(s)$ over $\mathscr{I}_s$:

$$\xi(s)=l\{-\zeta_0(s)+\alpha\zeta_1(s)+\beta\zeta_2(s)+\zeta_3(s)\}, \quad -1<\alpha<\beta<1 \tag{28}$$

with respect to a local co-ordinate system as in Figure 6. Parameters α and β must be selected such that inverse mapping $s(\xi)$ exists over $\mathscr{I}_\xi \overset{\text{def}}{=} [-l, l]$ and be represented as

$$s(\xi)=a+b\sqrt{l-\xi}+o(l-\xi) \tag{29}$$

It is straightforward proving that $\alpha=\frac{1}{9}$ and $\beta=\frac{7}{9}$ is the unique pair that satisfies requirements (28) and (29), for being

$$s(\xi)=1-\sqrt{\frac{2}{l}}\sqrt{l-\xi} \tag{30}$$

***T stands for T_j as well as for T_{tip}.

DOI: 10.1002/nme

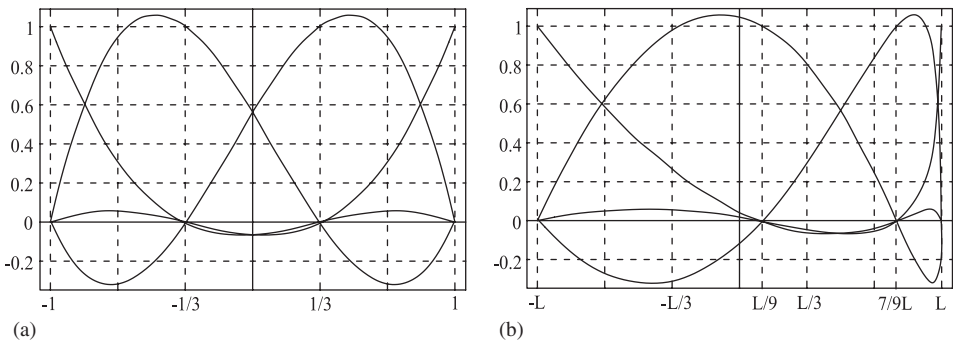

Figure 6. (a) Lagrangian shape functions over $\mathscr{I}_s$; and (b) modified quarter point shape functions over $\mathscr{I}_\xi$.

In view of result (30), the approximation of opening and sliding along the crack $\mathbf{w}$ at the crack tip can be achieved through shape functions basis $\boldsymbol{\Phi} \stackrel{\text{def}}{=} \{\varphi_j(\xi) = \zeta_j(s(\xi))\}$ with $\xi \in \mathscr{I}_\xi$, as usual for isoparametric elements, which have the following form:

$$\varphi_j(\xi) = \sum_{i=0}^{3} a_{ij}(l-\xi)^{i/2}, \quad a_{0j} \neq 0 \quad \text{if and only if } j = 3 \tag{31}$$

The constraint $\mathbf{w}(l) = 0$ at the crack tip forces the approximation of $\mathbf{w}$ to read:

$$\mathbf{w}(\xi) = \sum_{j=0}^{2} \mathbf{w}_j \varphi_j(\xi) \tag{32}$$

Result (31) induces to approximation (32) the theoretical asymptotic square root behaviour. It has recently been shown [30] that the linear coefficient of the asymptotic expansion of opening and sliding $\mathbf{w}$ at the crack tip vanishes. Compatibility with respect to this outcome produces an unsatisfied constraint for approximation (32):

$$\sum_{j=0}^{2} a_{2j}\mathbf{w}_j = 0 \tag{33}$$

A possible way to enforce constraint (33) is approximating crack opening and sliding $\mathbf{w}$ by means of shape functions basis $\tilde{\boldsymbol{\Phi}} \stackrel{\text{def}}{=} \{\tilde{\varphi}_j(\xi) = \tilde{\zeta}_j(s(\xi))\}$ with $\xi \in \mathscr{I}_\xi$ such that:

$$a_{2j} = 0 \quad \forall j \tag{34}$$

and $s(\xi)$ defined by (29). Constraint (34) is compatible with a polynomial shape function basis $\tilde{\boldsymbol{\Upsilon}}$ of degree increased by one with respect to $\boldsymbol{\Upsilon}$: consider partition $\mathscr{P}$ and fourth-order polynomial $m(s)$ such that $m(P_i) = 0$. Assume $\tilde{\boldsymbol{\Upsilon}} \stackrel{\text{def}}{=} \{\tilde{\zeta}_j(s) = \zeta_j(s) + \kappa_j m(s),\ j = 0, 1, 2, 3\}$ with $\kappa_j \in \mathbb{R}$, $s \in \mathscr{I}_s$. Note that $\tilde{\zeta}_j(P_i) = \delta_{ij}$. Shape functions $\tilde{\varphi}_j(\xi) = \tilde{\zeta}_j(s(\xi))$ are defined by means of $s(\xi)$ as in (29): coefficient κ_j can be uniquely evaluated in order to satisfy constraint (34) for any $\tilde{\varphi}_j(\xi)$. Incompatibility of constraints (34) and mapping (30) causes the loss of any iso-parametric formulation, in the sense that $\kappa_j \neq 0$ so that functions $\tilde{\zeta}_j$ and ζ_j can never coincide.

DOI: 10.1002/nme

In conclusion, approximation of opening and sliding along the crack $\mathbf{w}$ at the crack tip reads:

$$\mathbf{w}(\xi) = \sum_{j=0}^{2} \mathbf{w}_j \tilde{\varphi}_j(\xi), \quad \tilde{\varphi}_j(\xi) = \sum_{i=0}^{4} a_{ij}(l-\xi)^{i/2}$$
$$a_{0j} \neq 0 \quad \text{if and only if } j=3, \quad a_{2j}=0 \quad \forall j \tag{35}$$

with $\xi \in \mathscr{I}_\xi$. Basis $\tilde{\mathbf{\Phi}}$ is depicted in Figure 6(b) and printed in Appendix A.

4. ANALYTICAL INTEGRATIONS FOR CBEM AND BIRs

4.1. Problem formulation

In their vectorial forms, integral (13) as well as the inner integral[†††] in (14) take the form:

$$\mathbf{F}_{rs}(\mathbf{x}) \stackrel{\text{def}}{=} \int_{\Gamma_s} \mathbf{G}_{rs}(\mathbf{r})\psi_h(\mathbf{y})\,\mathrm{d}\Gamma_y \mathbb{1} = \int_{\mathscr{T}_h} \mathbf{G}_{rs}(\mathbf{r})\,\psi_h(\mathbf{y})\,\mathrm{d}\Gamma_y \mathbb{1} = \sum_{T\in\mathscr{T}_h} \mathbf{F}_{rs}(\mathbf{x}, T)$$

having defined with $\mathbb{1}$ the identity matrix,

$$\mathbf{F}_{rs}(\mathbf{x}, T) \stackrel{\text{def}}{=} \int_T \mathbf{G}_{rs}(\mathbf{r})\tilde{\varphi}_n(\xi_1)\,\mathrm{d}\xi_1 \mathbb{1} \tag{36}$$

and $\mathbf{r} = \mathbf{x} - \mathbf{y}(\xi_1)$. When $T = T_j$ integral (36) can be analytically solved according to [6]. When $T = T_{\text{tip}}$ split $\tilde{\varphi}_n(\xi_1)$ defined in Equation (35) in the sum:

$$\tilde{\varphi}_n(\xi_1) = \tilde{\varphi}_n^{\surd}(\xi_1) + a_{4n}(l-\xi_1)^2, \quad n=0,1,2 \tag{37}$$

where:

$$\tilde{\varphi}_n^{\surd}(\xi_1) = \sum_{i=1,3} a_{in}(l-\xi_1)^{i/2}, \quad n=0,1,2 \tag{38}$$

Integral (36) splits as well in the sum of two factors: the latter can be analytically solved according to [6], the former:

$$\mathbf{F}_{rs}(\mathbf{x}, T_{\text{tip}}) = \int_{T_{\text{tip}}} \mathbf{G}_{rs}(\mathbf{r})\,\tilde{\varphi}_n^{\surd}(\xi_1)\,\mathrm{d}\xi_1 \mathbb{1} \tag{39}$$

can be tackled as follows.

Consider local reference $\{0, \boldsymbol{\xi}\}$ over $T = T_{\text{tip}}$ and denote, with abuse of notation, with $\xi_1 = \xi_1(\mathbf{y})$, $\xi_2 = \xi_2(\mathbf{y}) = 0$, $\eta_1 = \xi_1(\mathbf{x})$, $\eta_2 = \xi_2(\mathbf{x})$ (Figure 7).

Noting that

$$\sqrt{l-\xi_1} = \sqrt{d_1 + r_1}, \quad (l-\xi_1)^{3/2} = (d_1+r_1)\sqrt{d_1+r_1}$$

Equation (38) can be written as

$$\tilde{\varphi}_n^{\surd}(\xi_1) = \mathbf{r}_1^{\mathsf{T}}\mathbf{X}\mathbf{a}_n\sqrt{d_1+r_1}, \quad n=0,1,2 \tag{40}$$

[†††]For the sake of brevity, here and in the following term 'integral' refers to CPV and HFP as well.

DOI: 10.1002/nme

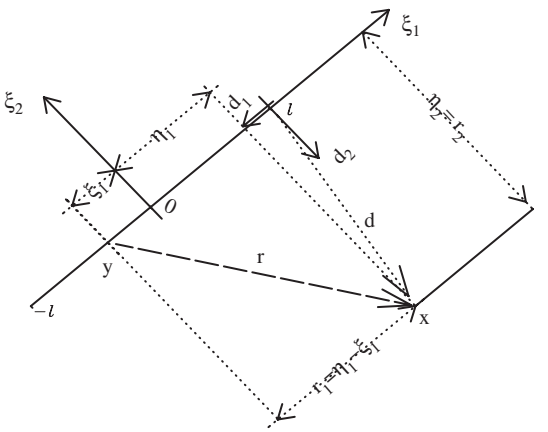

Figure 7. Notation.

where

$$\mathbf{r}_1^{\mathsf{T}} = [1, r_1], \quad \mathbf{X} = \begin{bmatrix} 1 & d_1 \\ 0 & 1 \end{bmatrix}, \quad \mathbf{a}_n = \begin{bmatrix} a_{1n} \\ a_{3n} \end{bmatrix} \tag{41}$$

By a trivial variable change, Equation (36) becomes:

$$\mathbf{F}_{rs}(\mathbf{x}, T_{\text{tip}}) = \int_{\eta_1 - l}^{\eta_1 + l} \mathbf{G}_{rs}(\mathbf{r}) \begin{bmatrix} \mathbf{r}_1^{\mathsf{T}} & 0 \\ 0 & \mathbf{r}_1^{\mathsf{T}} \end{bmatrix} \sqrt{d_1 + r_1}\, \mathrm{d}r_1 \Bigg|_{r_2 = x_2} \begin{bmatrix} \mathbf{X}\mathbf{a}_n & 0 \\ 0 & \mathbf{X}\mathbf{a}_n \end{bmatrix} \tag{42}$$

In conclusion, to perform the inner integral over panel T_{tip} one only needs to evaluate the following one:

$$\mathbf{K}_{rs}(\mathbf{x}, T_{\text{tip}}) = \int_{\eta_1 - l}^{\eta_1 + l} \mathbf{G}_{rs}(\mathbf{r}) \begin{bmatrix} \mathbf{r}_1^{\mathsf{T}} & 0 \\ 0 & \mathbf{r}_1^{\mathsf{T}} \end{bmatrix} \sqrt{d_1 + r_1}\, \mathrm{d}r_1 \Bigg|_{r_2 = x_2} \tag{43}$$

which depends on the kernel $\mathbf{G}_{rs}$ and on the position of the point $\mathbf{x}$ with respect to panel T_{tip}. Kernels $\mathbf{G}_{up}(\mathbf{x} - \mathbf{y}, \mathbf{l}(\mathbf{y}))$ and $\mathbf{G}_{pp}(\mathbf{x} - \mathbf{y}, \mathbf{n}(\mathbf{x}), \mathbf{l}(\mathbf{y}))$ are *singular with respect to* $\mathbf{y}$ depending on the position of $\mathbf{x}$ with respect to T_{tip}. Items $\mathbf{x} \notin \bar{T}_{\text{tip}}$—that leads to a Lebesgue integral—and $\mathbf{x} \in T_{\text{tip}}$—that leads to a finite part of Hadamard—will be accordingly separately analysed.

4.2. Lebesgue integrals

By substituting expressions of kernels $\mathbf{G}_{rs}$—see [6, Appendix A]—into integral (43), algebraic manipulations lead to the following basic integrals, with $k \in \mathbb{N}$:

$$\int_{\eta_1 - l}^{\eta_1 + l} \frac{r_1^k}{r^2} \sqrt{d_1 + r_1}\, \mathrm{d}r_1, \quad \int_{\eta_1 - l}^{\eta_1 + l} \frac{r_1^k}{r^4} \sqrt{d_1 + r_1}\, \mathrm{d}r_1, \quad \int_{\eta_1 - l}^{\eta_1 + l} \frac{r_1^k}{r^6} \sqrt{d_1 + r_1}\, \mathrm{d}r_1$$

DOI: 10.1002/nme

They have been analytically solved—results are collected in Appendix B—when $\mathbf{x} \notin \bar{T}_{\text{tip}}$. Taking apart all common terms, setting $\mathbf{d} = \{d_1, d_2\}$, $d_1 = l - \eta_1$, $d_2 = -\eta_2$, and $\alpha = \sqrt{d_1 + r_1}$, the following compact expressions are the outcome for integrals (43), having defined $\eta_1 = \xi_1(\mathbf{x})$ and $\eta_2 = \xi_2(\mathbf{x})$ according to Figure 7:

$$\mathbf{K}_{up}(\mathbf{x}, T_{\text{tip}}) = \frac{1}{16\pi}\frac{1}{1-\nu}\left[h(\mathbf{d};\alpha)\mathbf{L}_{up}(\mathbf{d}) + \vartheta(\mathbf{d};\alpha)\mathbf{A}_{up}(\mathbf{d}) + \frac{\alpha}{r^2}\mathbf{S}_{up}(\mathbf{d};r_1) + \alpha\mathbf{P}_{up}(\mathbf{d};r_1)\right]_{r_1=\eta_1-l}^{r_1=\eta_1+l} \tag{44}$$

$$\mathbf{K}_{pp}(\mathbf{x}, T_{\text{tip}}) = \frac{G}{16\pi}\frac{1}{1-\nu}\left[h(\mathbf{d};\alpha)\mathbf{L}_{pp}(\mathbf{d}) + \vartheta(\mathbf{d};\alpha)\mathbf{A}_{pp}(\mathbf{d}) + \frac{\alpha}{r^2}\mathbf{S}_{pp}(\mathbf{d};r_1) + \frac{\alpha}{r^4}\mathbf{H}_{pp}(\mathbf{d};r_1) + \alpha\mathbf{P}_{pp}(\mathbf{d};r_1)\right]_{r_1=\eta_1-l}^{r_1=\eta_1+l} \tag{45}$$

where $\mathbf{L}_{rp}$, $\mathbf{A}_{rp}$, $\mathbf{P}_{rp}$, $\mathbf{S}_{rp}$, $\mathbf{H}_{pp}$ with $r = u, p$ are suitable matrices that are collected in Appendix C with reference to shape functions (38).

4.2.1. Particular cases: strong singularity analysis. As a particular instance of Lebesgue integral, assume $\mathbf{x} \notin T_{\text{tip}}$, with $\eta_2 = 0$ (see Figure 8). The expression of *strongly singular kernel* $\mathbf{G}_{up}$ simplifies as

$$\mathbf{G}_{up}(\mathbf{r}, \mathbf{l}(\mathbf{y})) = -\frac{1}{4\pi}\frac{1-2\nu}{1-\nu}\begin{bmatrix} 0 & 1 \\ -1 & 0 \end{bmatrix}\frac{1}{r_1} \tag{46}$$

Integral (43) simplifies as well:

$$\mathbf{K}_{up}(\mathbf{x}, T_{\text{tip}}) = -\frac{1}{4\pi}\frac{1-2\nu}{1-\nu}\begin{bmatrix} 0 & 1 \\ -1 & 0 \end{bmatrix}\int_{\eta_1-l}^{\eta_1+l}\frac{\sqrt{d_1+r_1}}{r_1}\begin{bmatrix} \mathbf{r}_1^{\mathsf{T}} & 0 \\ 0 & \mathbf{r}_1^{\mathsf{T}} \end{bmatrix}\mathrm{d}r_1$$

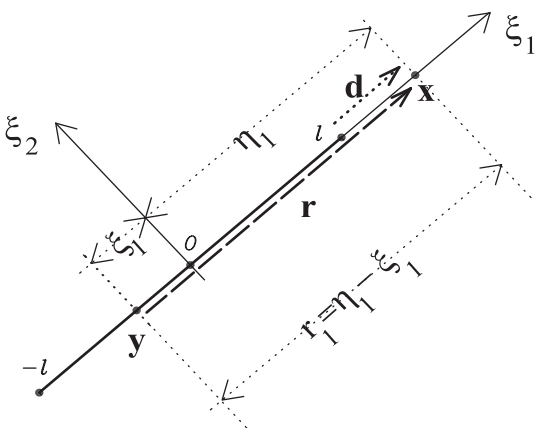

Figure 8. $\mathbf{x} \notin T_{\text{tip}}$, but $\eta_2 = 0$.

DOI: 10.1002/nme

and for shape functions (38)—for which $\mathbf{r}_1^{\mathsf{T}} = [1, r_1]$—it is straightforward to obtain:

$$\mathbf{K}_{up}(\mathbf{x}, T_{\text{tip}}) = -\frac{1}{4\pi}\frac{1-2\nu}{1-\nu}\begin{bmatrix} 0 & \mathbf{r}_{up}^{\mathsf{T}}(\mathbf{x}) \\ -\mathbf{r}_{up}^{\mathsf{T}}(\mathbf{x}) & 0 \end{bmatrix} \tag{47}$$

where

$$\mathbf{r}_{up}^{\mathsf{T}}(\mathbf{x}) = \left[2\left(\alpha - \sqrt{d_1}\,\text{arctanh}\left(\frac{\alpha}{\sqrt{d_1}}\right)\right), \frac{2\alpha^3}{3}\right]_{r_1=\eta_1-l}^{r_1=\eta_1+l}$$

having set $d_1 = l - \eta_1$, $\alpha = \sqrt{d_1 + r_1}$ with functions $\sqrt{\cdot} : \mathbb{R} \to \mathbb{C}$ and $\text{arctanh}(\cdot) : \mathbb{C} \to \mathbb{C}$.

Result (47) can be deduced by the—more general—limit to the boundary approach, by means of the limit:

$$\mathbf{K}_{up}(\mathbf{x}, T_{\text{tip}}) = \lim_{\mathbf{z} \to \mathbf{x} \notin T_{\text{tip}}} \mathbf{K}_{up}(\mathbf{z}, T_{\text{tip}}) \tag{48}$$

depicted in Figure 9. Set $\mathbf{d} = \{d_1, d_2\}$, $d_1 = l - \eta_1$, $d_2 = -\eta_2$, $\alpha = \sqrt{d_1 + r_1}$, $\eta_1 = \xi_1(\mathbf{z})$, and $\eta_2 = \xi_2(\mathbf{z})$. According to Equation (44),

$$\mathbf{K}_{up}(\mathbf{z}, T_{\text{tip}}) = \frac{h(\mathbf{d}; \sqrt{2l})\mathbf{L}_{up}(\mathbf{d}) + [\vartheta(\mathbf{d}; \sqrt{2l}) - \pi\,\text{sgn}(d_2)]\mathbf{A}_{up}(\mathbf{d}) + \sqrt{2l}\mathbf{P}_{up}(\mathbf{d}; \eta_1 + l)}{16\pi(1-\nu)} \tag{49}$$

Assume $d_1 < 0$—as in Figure 9: with reference to Appendix B, $\lim_{d_2 \to 0} a(\mathbf{d}) = 0$ and $\lim_{d_2 \to 0} b(\mathbf{d}) = -\text{sgn}(d_2)\sqrt{|\mathbf{d}|}$ have the following implications on $\mathbf{K}_{up}(\mathbf{z}, T_{\text{tip}})$—see also Equations (20) and (25):

$$\lim_{d_2 \to 0} h(\mathbf{d}; \sqrt{2l})\Big|_{d_1 < 0} = 0$$

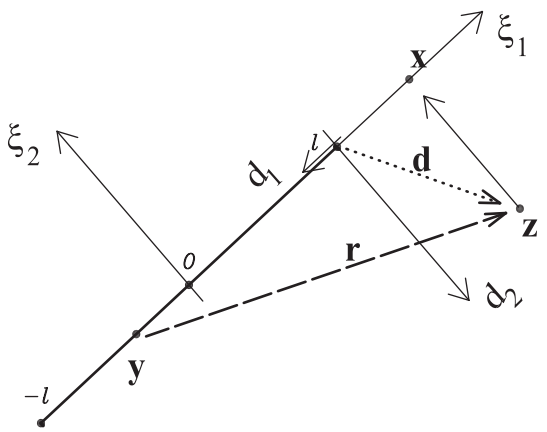

Figure 9. Limit to the boundary.

DOI: 10.1002/nme

$$\lim_{d_2\to 0}\vartheta(\mathbf{d};\sqrt{2l})\bigg|_{d_1<0}=2\,\mathrm{sgn}(d_2)\arctan\left(\frac{\sqrt{|\mathbf{d}|}}{\sqrt{2l}}\right)$$

$$\lim_{d_2\to 0}\mathbf{A}_{up}(\mathbf{d})\bigg|_{d_1<0}=4\,(1-2\nu)\mathrm{sgn}(d_2)\sqrt{|\mathbf{d}|}\begin{bmatrix}\{0,0\} & \{-1,0\}\\ \{1,0\} & \{0,0\}\end{bmatrix}$$

$$\lim_{d_2\to 0}\mathbf{P}_{up}(\mathbf{d};\eta_1+l)\bigg|_{d_1<0}=8(1-2\nu)\begin{bmatrix}\{0,0\} & \left\{-1,-\dfrac{\alpha^2}{3}\right\}\\ \left\{1,\dfrac{\alpha^2}{3}\right\} & \{0,0\}\end{bmatrix}$$

It comes out therefore from Equation (49):

$$\mathbf{K}_{up}(\mathbf{x},T_{\mathrm{tip}})|_{\substack{\eta_1>l\\ \eta_2=0}}=\frac{(1-2\nu)}{4\pi(1-\nu)}\left\{\left[2\arctan\left(\frac{\sqrt{|\mathbf{d}|}}{\sqrt{2l}}\right)-\pi\right]\sqrt{|\mathbf{d}|}+2\sqrt{2l}\right\}\begin{bmatrix}\{0,0\} & \left\{-1,-\dfrac{\alpha^2}{3}\right\}\\ \left\{1,\dfrac{\alpha^2}{3}\right\} & \{0,0\}\end{bmatrix}\tag{50}$$

Assume $d_1>2l>0$: with reference to Appendix B, $\lim_{d_2\to 0}a(\mathbf{d})=\sqrt{|\mathbf{d}|}$ and $\lim_{d_2\to 0}b(\mathbf{d})=0$ have the following implications on $\mathbf{K}_{up}(\mathbf{z},T_{\mathrm{tip}})$—see also Equations (18), (19) and (25):

$$\lim_{d_2\to 0}h(\mathbf{d};\sqrt{2l})\bigg|_{d_1>0}=2\log\frac{\sqrt{|\mathbf{d}|}+\sqrt{2l}}{\left|\sqrt{|\mathbf{d}|}-\sqrt{2l}\right|}$$

$$\lim_{d_2\to 0}\vartheta(\mathbf{d};\sqrt{2l})\bigg|_{d_1>2l}=\pi\,\mathrm{sgn}(d_2)$$

$$\lim_{d_2\to 0}\mathbf{A}_{up}(\mathbf{d})\bigg|_{d_1>0}=8\,(1-\nu)\sqrt{|\mathbf{d}|}\begin{bmatrix}\{1,0\} & \{0,0\}\\ \{0,0\} & \{1,0\}\end{bmatrix}$$

$$\lim_{d_2\to 0}\mathbf{L}_{up}(\mathbf{d};\eta_1+l)\bigg|_{d_1>0}=-2(1-2\nu)\sqrt{|\mathbf{d}|}\begin{bmatrix}\{0,0\} & \{-1,0\}\\ \{1,0\} & \{0,0\}\end{bmatrix}\tag{51}$$

$$\lim_{d_2\to 0}\mathbf{P}_{up}(\mathbf{d};\eta_1+l)\bigg|_{d_1>0}=8\,(1-2\nu)\begin{bmatrix}\{0,0\} & \left\{-1,-\dfrac{\alpha^2}{3}\right\}\\ \left\{1,\dfrac{\alpha^2}{3}\right\} & \{0,0\}\end{bmatrix}$$

DOI: 10.1002/nme

It comes out therefore from Equation (49):

$$\mathbf{K}_{up}(\mathbf{x}, T_{\text{tip}})|_{\substack{\eta_1<-l \\ \eta_2=0}} = \frac{(1-2\nu)}{4\pi(1-\nu)} \left\{ -\sqrt{|\mathbf{d}|}\log\frac{\sqrt{|\mathbf{d}|}+\sqrt{2l}}{\sqrt{|\mathbf{d}|}-\sqrt{2l}} + 2\sqrt{2l} \right\} \begin{bmatrix} \{0,0\} & \left\{-1, -\dfrac{\alpha^2}{3}\right\} \\ \left\{1, \dfrac{\alpha^2}{3}\right\} & \{0,0\} \end{bmatrix} \tag{52}$$

Equations (47), (50) and (52) are equivalent.

With the notable exception of Equation (51), limit process (48) applies also for $2l>d_1>0$, that is[‡‡‡] $\mathbf{x} \in T_{\text{tip}}$. For being:

$$\lim_{d_2 \to 0} \vartheta(\mathbf{d}; \sqrt{2l})\Big|_{0<d_1<2l} = 0$$

it comes out from Equation (49) for the case $\mathbf{x} \in T_{\text{tip}}$ not considered in Equation (47):

$$\mathbf{K}_{up}(\mathbf{x}, T_{\text{tip}})|_{\substack{-l<\eta_1<l \\ \eta_2=0}} = \frac{(1-2\nu)}{4\pi(1-\nu)} \left\{ -\sqrt{|\mathbf{d}|}\log\frac{\sqrt{|\mathbf{d}|}+\sqrt{2l}}{\sqrt{|\mathbf{d}|}-\sqrt{2l}} + 2\sqrt{2l} \right\} \begin{bmatrix} \{0,0\} & \left\{-1, -\dfrac{\alpha^2}{3}\right\} \\ \left\{1, \dfrac{\alpha^2}{3}\right\} & \{0,0\} \end{bmatrix}$$

$$-\frac{1}{2}\,\text{sgn}(d_2)\sqrt{|\mathbf{d}|} \begin{bmatrix} \{1,0\} & \{0,0\} \\ \{0,0\} & \{1,0\} \end{bmatrix} \tag{53}$$

4.2.2. Particular cases: hyper singularity analysis. As a particular instance of Lebesgue integral, assume $\mathbf{x} \notin T_{\text{tip}}$, with $\eta_2 = 0$ (see Figure 8). The *hyper singular kernel* takes the following expression:

$$\mathbf{G}_{pp}(\mathbf{r}, \mathbf{l}(\mathbf{y})) = \frac{G}{2\pi}\frac{1}{1-\nu} \begin{bmatrix} n_2 & n_1 \\ n_1 & n_2 \end{bmatrix} \frac{1}{r_1^2} \tag{54}$$

Integral (43) simplifies as well:

$$\mathbf{K}_{pp}(\mathbf{x}, T_{\text{tip}}) = \frac{G}{2\pi}\frac{1}{1-\nu} \begin{bmatrix} n_2 & n_1 \\ n_1 & n_2 \end{bmatrix} \int_{\eta_1-l}^{\eta_1+l} \frac{\sqrt{d_1+r_1}}{r_1^2} \begin{bmatrix} \mathbf{r}_1^{\mathsf{T}} & 0 \\ 0 & \mathbf{r}_1^{\mathsf{T}} \end{bmatrix} \mathrm{d}r_1$$

and for shape functions (38)—for which $\mathbf{r}_1^{\mathsf{T}} = [1, r_1]$—it is straightforward to obtain:

$$\mathbf{K}_{pp}(\mathbf{x}, T_{\text{tip}}) = \frac{G}{2\pi}\frac{1}{1-\nu} \begin{bmatrix} n_2 & n_1 \\ n_1 & n_2 \end{bmatrix} \begin{bmatrix} \mathbf{r}_{pp}^{\mathsf{T}}(\mathbf{x}) & 0 \\ 0 & \mathbf{r}_{pp}^{\mathsf{T}}(\mathbf{x}) \end{bmatrix} \tag{55}$$

[‡‡‡]In this case integral (43) does not exists (in fact, it must be considered in its nature of Cauchy's principal value as it will be seen in Section 4.3).

DOI: 10.1002/nme

where

$$\mathbf{r}_{pp}^{\mathsf{T}}(\mathbf{x}) = \left[-\frac{\sqrt{d_1}}{d_1} \operatorname{arctanh}\left(\frac{\alpha}{\sqrt{d_1}}\right) - \frac{\alpha}{r_1}, \quad -2\sqrt{d_1} \operatorname{arctanh}\left(\frac{\alpha}{\sqrt{d_1}}\right) + 2\alpha \right]_{r_1=\eta_1-l}^{r_1=\eta_1+l}$$

having set $d_1 = l - \eta_1$, $\alpha = \sqrt{d_1 + r_1}$ with functions $\sqrt{\cdot} : \mathbb{R} \to \mathbb{C}$ and $\operatorname{arctanh}(\cdot) : \mathbb{C} \to \mathbb{C}$.

Outcome (55) can be deduced and depicted in $\mathbb{R}$ making recourse to the—more general—limit to the boundary approach, by means of the limit:

$$\mathbf{K}_{pp}(\mathbf{x}, T_{\text{tip}}) = \lim_{\mathbf{z} \to \mathbf{x} \notin T_{\text{tip}}} \mathbf{K}_{pp}(\mathbf{z}, T_{\text{tip}}) \tag{56}$$

Set $\mathbf{d} = \{d_1, d_2\}$, $d_1 = l - \eta_1$, $d_2 = -\eta_2$, $\alpha = \sqrt{d_1 + r_1}$, $\eta_1 = \xi_1(\mathbf{z})$, and $\eta_2 = \xi_2(\mathbf{z})$. According to Equation (45),

$$\begin{aligned} \mathbf{K}_{pp}(\mathbf{z}, T_{\text{tip}}) = \frac{G}{16\pi(1-\nu)} \Bigg\{ & h(\mathbf{d}; \sqrt{2l}) \mathbf{L}_{pp}(\mathbf{d}) + [\vartheta(\mathbf{d}; \sqrt{2l}) - \pi \operatorname{sgn}(d_2)] \mathbf{A}_{pp}(\mathbf{d}) \\ & + \frac{\sqrt{2l}}{(\eta_1 + l)^2} \mathbf{S}_{pp}(\mathbf{d}; \eta_1 + l) + \frac{\sqrt{2l}}{(\eta_1 + l)^4} \mathbf{H}_{pp}(\mathbf{d}; \eta_1 + l) \\ & + \sqrt{2l} \mathbf{P}_{pp}(\mathbf{d}; \eta_1 + l) \Bigg\} \end{aligned} \tag{57}$$

Assume $d_1 < 0$—as in Figure 9: with reference to Appendix B, $\lim_{d_2 \to 0} a(\mathbf{d}) = 0$ and $\lim_{d_2 \to 0} b(\mathbf{d}) = -\operatorname{sgn}(d_2)\sqrt{|\mathbf{d}|}$ have the following implications on $\mathbf{K}_{pp}(\mathbf{z}, T_{\text{tip}})$—see also Equations (20) and (25):

$$\lim_{d_2 \to 0} h(\mathbf{d}; \sqrt{2l}) \Big|_{d_1 < 0} = 0$$

$$\lim_{d_2 \to 0} \vartheta(\mathbf{d}; \sqrt{2l}) \Big|_{d_1 < 0} = 2 \operatorname{sgn}(d_2) \arctan\left(\frac{\sqrt{|\mathbf{d}|}}{\sqrt{2l}}\right)$$

$$\lim_{d_2 \to 0} \mathbf{A}_{pp}(\mathbf{d}) \Big|_{d_1 < 0} = -2 \operatorname{sgn}(d_2) \frac{\sqrt{|\mathbf{d}|}}{|\mathbf{d}|} \begin{bmatrix} \{2n_2, -4n_2|\mathbf{d}|\} & \{2n_1, -4n_1|\mathbf{d}|\} \\ \{2n_1, -4n_1|\mathbf{d}|\} & \{2n_2, -4n_2|\mathbf{d}|\} \end{bmatrix}$$

$$\lim_{d_2 \to 0} \mathbf{H}_{pp}(\mathbf{d}; \eta_1 + l) \Big|_{d_1 < 0} = \mathbf{0}$$

$$\lim_{d_2 \to 0} \mathbf{S}_{pp}(\mathbf{d}; \eta_1 + l) \Big|_{d_1 < 0} = -8(\eta_1 + l) \begin{bmatrix} \{n_2, 0\} & \{n_1, 0\} \\ \{n_1, 0\} & \{n_2, 0\} \end{bmatrix}$$

$$\lim_{d_2 \to 0} \mathbf{P}_{pp}(\mathbf{d}; \eta_1 + l) \Big|_{d_1 < 0} = 16 \begin{bmatrix} \{0, n_2\} & \{0, n_1\} \\ \{0, n_1\} & \{0, n_2\} \end{bmatrix}$$

DOI: 10.1002/nme

It comes out therefore from Equation (57):

$$\mathbf{K}_{pp}(\mathbf{x}, T_{\text{tip}})|_{\substack{\eta_1>l \\ \eta_2=0}} = \frac{G}{16\pi(1-\nu)} \begin{bmatrix} n_2 & n_1 \\ n_1 & n_2 \end{bmatrix} \times \left\{ -2\left[2 \arctan \frac{\sqrt{|\mathbf{d}|}}{\sqrt{2l}} - \pi\right] \frac{\sqrt{|\mathbf{d}|}}{|\mathbf{d}|} \begin{bmatrix} \{2, -4|\mathbf{d}|\} & \{0,0\} \\ \{0,0\} & \{2, -4|\mathbf{d}|\} \end{bmatrix} - 8\frac{\sqrt{2l}}{\eta_1 + l} \begin{bmatrix} \{1,0\} & \{0,0\} \\ \{0,0\} & \{1,0\} \end{bmatrix} + 16\sqrt{2l} \begin{bmatrix} \{0,1\} & \{0,0\} \\ \{0,0\} & \{0,1\} \end{bmatrix} \right\} \tag{58}$$

Assume $d_1 > 2l > 0$: with reference to Appendix B, $\lim_{d_2\to 0} a(\mathbf{d}) = \sqrt{|\mathbf{d}|}$ and $\lim_{d_2\to 0} b(\mathbf{d}) = 0$ have the following implications on $\mathbf{K}_{pp}(\mathbf{z}, T_{\text{tip}})$—see also Equations (18), (19), and (25):

$$\lim_{d_2\to 0} h(\mathbf{d}; \sqrt{2l})\Big|_{d_1>0} = 2\log\frac{\sqrt{|\mathbf{d}|} + \sqrt{2l}}{|\sqrt{|\mathbf{d}|} - \sqrt{2l}|}$$

$$\lim_{d_2\to 0} \vartheta(\mathbf{d}; \sqrt{2l})\Big|_{d_1>2l} = \pi \operatorname{sgn}(d_2)$$

$$\lim_{d_2\to 0} \mathbf{A}_{pp}(\mathbf{d})\Big|_{d_1>0} = -8n_1\sqrt{|\mathbf{d}|} \begin{bmatrix} \left\{\frac{1}{|\mathbf{d}|}, 2\right\} & \{0,0\} \\ \{0,0\} & \{0,0\} \end{bmatrix}$$

$$\lim_{d_2\to 0} \mathbf{L}_{pp}(\mathbf{d}; \eta_1 + l)\Big|_{d_1>0} = -2\sqrt{|\mathbf{d}|} \begin{bmatrix} \left\{\frac{n_2}{|\mathbf{d}|}, 2n_2\right\} & \left\{\frac{n_1}{|\mathbf{d}|}, 2n_1\right\} \\ \left\{\frac{n_1}{|\mathbf{d}|}, 2n_1\right\} & \left\{\frac{n_2}{|\mathbf{d}|}, 2n_2\right\} \end{bmatrix} \tag{59}$$

$$\lim_{d_2\to 0} \mathbf{H}_{pp}(\mathbf{d}; \eta_1 + l)\Big|_{d_1>0} = \mathbf{0}$$

$$\lim_{d_2\to 0} \mathbf{S}_{pp}(\mathbf{d}; \eta_1 + l)\Big|_{d_1>0} = -8(\eta_1 + l) \begin{bmatrix} \{n_2, 0\} & \{n_1, 0\} \\ \{n_1, 0\} & \{n_2, 0\} \end{bmatrix}$$

$$\lim_{d_2\to 0} \mathbf{P}_{pp}(\mathbf{d}; \eta_1 + l)\Big|_{d_1>0} = 16 \begin{bmatrix} \{0, n_2\} & \{0, n_1\} \\ \{0, n_1\} & \{0, n_2\} \end{bmatrix}$$

DOI: 10.1002/nme

It comes out therefore from Equation (49):

$$\mathbf{K}_{pp}(\mathbf{x}, T_{\text{tip}})|_{\substack{\eta_1<-l \\ \eta_2=0}} = \frac{G}{16\pi(1-\nu)} \begin{bmatrix} n_2 & n_1 \\ n_1 & n_2 \end{bmatrix} \times \left\{ -4\sqrt{|\mathbf{d}|} \log \frac{\sqrt{|\mathbf{d}|}+\sqrt{2l}}{\left|\sqrt{|\mathbf{d}|}-\sqrt{2l}\right|} \begin{bmatrix} \left\{\frac{1}{|\mathbf{d}|}, 2\right\} & \{0,0\} \\ \{0,0\} & \left\{\frac{1}{|\mathbf{d}|}, 2\right\} \end{bmatrix} - 8\frac{\sqrt{2l}}{\eta_1+l} \begin{bmatrix} \{1,0\} & \{0,0\} \\ \{0,0\} & \{1,0\} \end{bmatrix} + 16\sqrt{2l} \begin{bmatrix} \{0,1\} & \{0,0\} \\ \{0,0\} & \{0,1\} \end{bmatrix} \right\} \tag{60}$$

Equations (55), (58) and (60) are equivalent.

With the notable exception of Equation (59), limit process (56) applies also for $2l>d_1>0$, that is[§§§] $\mathbf{x} \in T_{\text{tip}}$. For being:

$$\lim_{d_2 \to 0} \vartheta(\mathbf{d}; \sqrt{2l})\Big|_{0<d_1<2l} = 0$$

it comes out from Equation (57) for the case $\mathbf{x} \in T_{\text{tip}}$ not considered in Equation (55):

$$\mathbf{K}_{pp}(\mathbf{x}, T_{\text{tip}})|_{\substack{-l<\eta_1<l \\ \eta_2=0}} = \frac{G}{16\pi(1-\nu)} \begin{bmatrix} n_2 & n_1 \\ n_1 & n_2 \end{bmatrix} \times \left\{ -4\sqrt{|\mathbf{d}|} \log \frac{\sqrt{|\mathbf{d}|}+\sqrt{2l}}{\left|\sqrt{|\mathbf{d}|}-\sqrt{2l}\right|} \begin{bmatrix} \left\{\frac{1}{|\mathbf{d}|}, 2\right\} & \{0,0\} \\ \{0,0\} & \left\{\frac{1}{|\mathbf{d}|}, 2\right\} \end{bmatrix} - 8\frac{\sqrt{2l}}{\eta_1+l} \begin{bmatrix} \{1,0\} & \{0,0\} \\ \{0,0\} & \{1,0\} \end{bmatrix} + 16\sqrt{2l} \begin{bmatrix} \{0,1\} & \{0,0\} \\ \{0,0\} & \{0,1\} \end{bmatrix} \right\} + \frac{Gn_1}{2(1-\nu)} \operatorname{sgn}(d_2) \left(\sqrt{|\mathbf{d}|} \begin{bmatrix} \left\{\frac{1}{|\mathbf{d}|}, 2\right\} & \{0,0\} \\ \{0,0\} & \{0,0\} \end{bmatrix} \right) \tag{61}$$

[§§§] In this case integral (43) does not exists (in fact, it must be considered in its nature of Hadamard's finite part as it will be seen in Section 4.4).

DOI: 10.1002/nme

4.3. Cauchy principal value

Definition
The CPV [46] of the (usually) divergent integral $\int_{-\infty}^{+\infty}(\phi(t)/t)\,\mathrm{d}t$ is the finite quantity

$$\oint_{-\infty}^{+\infty}\frac{\phi(t)}{t}\,\mathrm{d}t := \lim_{\varepsilon\to 0^+}\left(\int_{-\infty}^{-\varepsilon}\frac{\phi(t)}{t}\,\mathrm{d}t + \int_{\varepsilon}^{+\infty}\frac{\phi(t)}{t}\,\mathrm{d}t\right)$$

When $\mathbf{x}\in T_{\text{tip}}$—i.e. $-l<\eta_1<l$—'integral' (43) is not defined in a Lebesgue sense. In view of identity (46) and of definition of $\mathbf{r}_1^{\mathsf{T}}$, it holds in fact:

$$\mathbf{K}_{up}(\mathbf{x}, T_{\text{tip}}) = -\frac{1}{4\pi}\frac{1-2\nu}{1-\nu}\begin{bmatrix}0 & 1\\ -1 & 0\end{bmatrix}\int_{\eta_1-l}^{\eta_1+l}\frac{\sqrt{d_1+r_1}}{r_1}\begin{bmatrix}[1,r_1] & 0\\ 0 & [1,r_1]\end{bmatrix}\mathrm{d}r_1$$

and function $\sqrt{d_1+r_1}/r_1$ is not integrable over any interval comprising $r_1=0$. It seems to be of interest to investigate the CPV

$$\oint\mathbf{K}_{up}(\mathbf{x}, T_{\text{tip}}) \overset{\text{def}}{=} -\frac{1}{4\pi}\frac{1-2\nu}{1-\nu}\begin{bmatrix}0 & 1\\ -1 & 0\end{bmatrix}\oint_{\eta_1-l}^{\eta_1+l}\frac{\sqrt{d_1+r_1}}{r_1}\begin{bmatrix}[1,r_1] & 0\\ 0 & [1,r_1]\end{bmatrix}\mathrm{d}r_1$$

that holds:

$$\begin{aligned}
\oint_{\eta_1-l}^{\eta_1+l}\frac{\sqrt{d_1+r_1}}{r_1}\,\mathrm{d}r_1 &= \lim_{\varepsilon\to 0^+}\left(\int_{\eta_1-l}^{-\varepsilon}\frac{\sqrt{d_1+r_1}}{r_1}\,\mathrm{d}r_1 + \int_{\varepsilon}^{\eta_1+l}\frac{\sqrt{d_1+r_1}}{r_1}\,\mathrm{d}r_1\right)\\
&= \lim_{\varepsilon\to 0^+}\left(\left[2\left(\alpha-\sqrt{d_1}\operatorname{arctanh}\left(\frac{\alpha}{\sqrt{d_1}}\right)\right)\right]_{r_1=\eta_1-l}^{r_1=-\varepsilon}\right.\\
&\quad\left.+\left[2\left(\alpha-\sqrt{d_1}\operatorname{arctanh}\left(\frac{\alpha}{\sqrt{d_1}}\right)\right)\right]_{r_1=\varepsilon}^{r_1=\eta_1+l}\right)\\
&= \left[2\left(\alpha-\sqrt{d_1}\operatorname{arctanh}\left(\frac{\alpha}{\sqrt{d_1}}\right)\right)\right]_{r_1=\eta_1-l}^{r_1=\eta_1+l}\\
&\quad-\lim_{\varepsilon\to 0^+}\left[2\left(\alpha-\sqrt{d_1}\operatorname{arctanh}\left(\frac{\alpha}{\sqrt{d_1}}\right)\right)\right]_{r_1=-\varepsilon}^{r_1=\varepsilon}\\
&= \left[2\left(\alpha-\sqrt{d_1}\operatorname{arctanh}\left(\frac{\alpha}{\sqrt{d_1}}\right)\right)\right]_{r_1=\eta_1-l}^{r_1=\eta_1+l}+O(\varepsilon)
\end{aligned}$$

DOI: 10.1002/nme

In view of outcome (53) it turns out that

$$\lim_{\mathbf{z}\to\mathbf{x}\in T_{\text{tip}}} \mathbf{K}_{up}(\mathbf{z}, T_{\text{tip}}) = \text{-}\mathbf{K}_{up}(\mathbf{x}, T_{\text{tip}}) - \frac{1}{2}\,\text{sgn}(d_2)\sqrt{l-\eta_1}\begin{bmatrix}\{1,0\} & \{0,0\}\\ \{0,0\} & \{1,0\}\end{bmatrix} \tag{62}$$

Result (62) was expected in view of its nature of discrete counterpart of the free-term for smooth boundaries. It holds in fact:

$$\begin{aligned}\lim_{\mathbf{z}\to\mathbf{x}\in T_{\text{tip}}} \mathbf{F}_{up}(\mathbf{z}, T_{\text{tip}}) &= \lim_{\mathbf{z}\to\mathbf{x}\in T_{\text{tip}}} \mathbf{K}_{up}(\mathbf{z}, T_{\text{tip}})\begin{bmatrix}\mathbf{X}\mathbf{a}_n & 0\\ 0 & \mathbf{X}\mathbf{a}_n\end{bmatrix}\\ &= \text{-}\mathbf{K}_{up}(\mathbf{x}, T_{\text{tip}})\begin{bmatrix}\mathbf{X}\mathbf{a}_n & 0\\ 0 & \mathbf{X}\mathbf{a}_n\end{bmatrix} - \frac{1}{2}\,\text{sgn}(d_2)\sqrt{l-\eta_1}\\ &\quad\times\begin{bmatrix}\{1,0\} & \{0,0\}\\ \{0,0\} & \{1,0\}\end{bmatrix}\begin{bmatrix}\mathbf{X}\mathbf{a}_n & 0\\ 0 & \mathbf{X}\mathbf{a}_n\end{bmatrix}\\ &= \text{-}\mathbf{F}_{up}(\mathbf{x}, T_{\text{tip}}) - \frac{1}{2}\,\text{sgn}(d_2)\tilde{\varphi}_n^{\surd}(\eta_1)\mathbb{1}\end{aligned} \tag{63}$$

with $\mathbf{F}_{up}$ defined by Equation (42), $\text{-}\mathbf{F}_{up}$ defined by comparison with $\text{-}\mathbf{K}_{up}$, $\tilde{\varphi}_n^{\surd}(\eta_1)$ defined in Equation (38), and with $\mathbb{1}$ denoting the identity matrix.

There is a sound mechanical meaning in the last identity: in view of the factor $\text{sgn}(d_2)$, limit (62) takes two different values depending on the direction of the limit process with respect to the normal at T_{tip}. Accordingly, $\mathbf{F}_{up}(\mathbf{x}, T_{\text{tip}})$ as a function of $\mathbf{x}$ shows a discontinuity when (and only when) $\mathbf{x}\in T_{\text{tip}}$. Since $\mathbf{F}_{up}$ represents the displacement field at point $\mathbf{x}$, a discontinuity across T_{tip}, i.e. a displacement jump between the two lips of the crack, models crack opening.

4.4. Hadamard's finite part

Definition 1
Let $\varepsilon\to I(\varepsilon)$ denote a complex-valued function which is continuous in $(0, \varepsilon_0)$ and assume that

$$I(\varepsilon) = I_0 + I_1\log(\varepsilon) + \sum_{j=2}^{m} I_j\varepsilon^{1-j} + o(1); \quad \varepsilon\to 0$$

where $I_j\in\mathbb{C}$. Then I_0 is called the finite part of $I(\varepsilon)$. In dealing with integrals, the finite part I_0 of a (usually) divergent integral $\int_{-\infty}^{+\infty}\phi(t)\,\mathrm{d}t$ is denoted by the symbol $\text{-}\!\!\!\!\!\int_{-\infty}^{+\infty}\phi(t)\,\mathrm{d}t$.

When $\mathbf{x}\in T_{\text{tip}}$—i.e. $-l<\eta_1<l$—'integral' (43) is not defined in a Lebesgue sense. In view of identity (54) and of definition of $\mathbf{r}_1^{\mathsf{T}}$, it holds in fact:

$$\mathbf{K}_{pp}(\mathbf{x}, T_{\text{tip}}) = \frac{G}{2\pi}\frac{1}{1-\nu}\begin{bmatrix}n_2 & n_1\\ n_1 & n_2\end{bmatrix}\int_{\eta_1-l}^{\eta_1+l}\frac{\sqrt{d_1+r_1}}{r_1^2}\begin{bmatrix}[1,r_1] & 0\\ 0 & [1,r_1]\end{bmatrix}\mathrm{d}r_1$$

DOI: 10.1002/nme

and function $\sqrt{d_1+r_1}/r_1^2$ is not integrable over any interval comprising $r_1=0$. It seems to be of interest to investigate the finite part of Hadamard:

$$\mathbb{\mathbf{K}}_{pp}(\mathbf{x}, T_{\text{tip}}) \stackrel{\text{def}}{=} \frac{G}{2\pi}\frac{1}{1-\nu}\begin{bmatrix} n_2 & n_1 \\ n_1 & n_2 \end{bmatrix} \mathbb{\int}_{\eta_1-l}^{\eta_1+l} \frac{\sqrt{d_1+r_1}}{r_1^2}\begin{bmatrix} [1, r_1] & 0 \\ 0 & [1, r_1] \end{bmatrix} \mathrm{d}r_1$$

Results obtained in Section 4.3 can be exploited to solve $\mathbb{\int}_{\eta_1-l}^{\eta_1+l}(\sqrt{d_1+r_1}/r_1)\,\mathrm{d}r_1$. The remaining term holds:

$$\begin{aligned}
&\lim_{\varepsilon\to 0^+}\left(\int_{\eta_1-l}^{-\varepsilon}\frac{\sqrt{d_1+r_1}}{r_1^2}\,\mathrm{d}r_1+\int_{\varepsilon}^{\eta_1+l}\frac{\sqrt{d_1+r_1}}{r_1^2}\,\mathrm{d}r_1\right)\\
&\quad=\lim_{\varepsilon\to 0^+}\left(\left[-\frac{\alpha}{r_1}-\frac{\sqrt{d_1}}{d_1}\operatorname{arctanh}\frac{\alpha}{\sqrt{d_1}}\right]_{r_1=\eta_1-l}^{r_1=-\varepsilon}+\left[-\frac{\alpha}{r_1}-\frac{\sqrt{d_1}}{d_1}\operatorname{arctanh}\frac{\alpha}{\sqrt{d_1}}\right]_{r_1=\varepsilon}^{r_1=\eta_1+l}\right)\\
&\quad=\left[-\frac{\alpha}{r_1}-\frac{\sqrt{d_1}}{d_1}\operatorname{arctanh}\frac{\alpha}{\sqrt{d_1}}\right]_{r_1=\eta_1-l}^{r_1=\eta_1+l}-\lim_{\varepsilon\to 0^+}\left[-\frac{\alpha}{r_1}-\frac{\sqrt{d_1}}{d_1}\operatorname{arctanh}\frac{\alpha}{\sqrt{d_1}}\right]_{r_1=-\varepsilon}^{r_1=\varepsilon}\\
&\quad=\left[-\frac{\alpha}{r_1}-\frac{\sqrt{d_1}}{d_1}\operatorname{arctanh}\frac{\alpha}{\sqrt{d_1}}\right]_{r_1=\eta_1-l}^{r_1=\eta_1+l}-\frac{2\sqrt{d_1}}{\varepsilon}+O(\varepsilon)
\end{aligned}$$

By definition,

$$\mathbb{\int}_{\eta_1-l}^{\eta_1+l}\frac{\sqrt{d_1+r_1}}{r_1^2}\,\mathrm{d}r_1=\left[-\frac{\alpha}{r_1}-\frac{\sqrt{d_1}}{d_1}\operatorname{arctanh}\frac{\alpha}{\sqrt{d_1}}\right]_{r_1=\eta_1-l}^{r_1=\eta_1+l}$$

In view of outcome (61) it turns out that

$$\lim_{\mathbf{z}\to\mathbf{x}\in T_{\text{tip}}}\mathbf{K}_{pp}(\mathbf{z}, T_{\text{tip}})=\mathbb{\mathbf{K}}_{pp}(\mathbf{x}, T_{\text{tip}})+\frac{Gn_1}{2(1-\nu)}\operatorname{sgn}(d_2)\sqrt{|\mathbf{d}|}\begin{bmatrix}\left\{\dfrac{1}{|\mathbf{d}|}, 2\right\} & \{0,0\}\\ \{0,0\} & \{0,0\}\end{bmatrix} \tag{64}$$

The same path of reasoning of Section 4.3 permits to infer a sound mechanical meaning to identity (64): in view of the factor $\operatorname{sgn}(d_2)$, limit (64) takes two different values depending on the direction of the limit process with respect to the normal $\mathbf{n}_{\text{tip}}(\mathbf{x})$ at T_{tip}. Accordingly, $\mathbf{F}_{pp}(\mathbf{x}, T_{\text{tip}})$ as a function of $\mathbf{x}$ shows a discontinuity when (and only when) $\mathbf{x}\in T_{\text{tip}}$. Since $\mathbf{F}_{pp}$ represents the traction field at point $\mathbf{x}$ across a surface of normal $\mathbf{n}(\mathbf{x})$, a discontinuity across T_{tip} may arise if and only if $n_1\neq 0$, that is, if $\mathbf{n}(\mathbf{x})$ differs from the normal $\mathbf{n}_{\text{tip}}(\mathbf{x})$ at T_{tip}.

In other words, the term:

$$\mathbf{D}_{pp}(\mathbf{x}, T_{\text{tip}})\stackrel{\text{def}}{=}\frac{Gn_1}{2(1-\nu)}\operatorname{sgn}(d_2)\left(\sqrt{|\mathbf{d}|}\begin{bmatrix}\left\{\dfrac{1}{|\mathbf{d}|}, 2\right\} & \{0,0\}\\ \{0,0\} & \{0,0\}\end{bmatrix}\right) \tag{65}$$

DOI: 10.1002/nme

plays the role of a free-term coming out the hypersingular kernel in the traction equation. It is evident that $\mathbf{D}_{pp}$ depends on the selected direction $\mathbf{n}(\mathbf{x})$ at point $\mathbf{x} \in T_{\text{tip}}$: when it is taken as the outward normal at $\mathbf{x}$, that is $\mathbf{n}(\mathbf{x}) = \mathbf{e}_2$, then $\mathbf{D}_{pp}$ vanishes and the free term in the traction equation is solely due to the strongly singular kernel. On the contrary, when the traction is sought with respect to a direction $\mathbf{n}(\mathbf{x})$ which differs from the normal at $\mathbf{x}$, then the hypersingular kernel contributes to the free term even on smooth boundaries. Contributions by the hypersingular kernel have been observed in literature in [47, 17] for the hypersingular BIE for displacement derivatives and in [10, 18] in the framework of potential theory, when the boundary curvature and the tangent vector to the boundary are not smooth. Free term (65) has a very different nature: a wide discussion on such a contribution will be the subject of a further publication.

Outcomes (63) and (64) particularizes to shape functions (38) a well-known result of distribution theory [48], namely the application of the trace operator to the representation formulae of elasticity.[¶¶¶] Following [7], the strongly singular and hypersingular integrals can be expressed by means of discontinuity jumps (also named 'free terms') of these integrals on the boundary summed with the values of the integrals on the boundary existing only in the sense of CPV or in the sense of Hadamard's finite part. By exploiting Green's functions properties, the commutativity of the two operations of traction and trace was proved [7], thus showing the consistency of several different approaches of derivations of the BIEs [9, 13, 14, 17].

4.5. On the computational cost of analytical integrations

The interest in analytical integrations is not limited to computational efficiency; nevertheless, 'measuring' the computational cost of their implementation can be of use. A key point to this aim is envisaging a unit of measurement independent on the computing machine, on the implemented code, on the programming language and also on the compiler: a very hard task to cope with. In this note, the computational cost $\mu(\mathbf{G}_{rs})$ of analytical integrations (43) has been measured[‖‖‖] by the number of evaluations of kernel $\mathbf{G}_{rs}$:

$$\mu(\mathbf{G}_{rs}) = \frac{\mathbf{K}_{rs}(\mathbf{x}, T_{\text{tip}}) \text{ elapsed time}}{\mathbf{G}_{rs} \text{ elapsed time}} \tag{66}$$

Results are collected in Table II. Measure (66) can be significantly related with the number of nodes $n_{\mathbf{Q}}(\mathbf{x})$ of the quadrature rule $\mathbf{Q}_{rs}(\mathbf{x}, T_{\text{tip}})$ eventually used to approximate integral (43), under the assumption that all computational time relies on kernels evaluation. Obviously, comparisons must be made with respect to a target accuracy

$$\zeta(\mathbf{x}) = \left\| \frac{\mathbf{Q}_{rs}(\mathbf{x}, T_{\text{tip}}) - \mathbf{K}_{rs}(\mathbf{x}, T_{\text{tip}})}{\mathbf{K}_{rs}(\mathbf{x}, T_{\text{tip}})} \right\|$$

whose amount and whose dependency on the field point $\mathbf{x}$ are intimately related to the notion of η-admissibility in fast integral operators; a discussion on this topic is far beyond the purpose of the present note, in which a fixed accuracy $\zeta = 10^{-8}$ has been selected. In Figures 10–13 the number of nodes $n_{\text{Gauss}}(\mathbf{x})$ required to reach accuracy ζ for a Gauss quadrature rule is mapped with reference

[¶¶¶] Somigliana's and traction identities.

[‖‖‖] Such a measure should not depend on the hardware, but merely on the implementation of kernel and analytical integrations.

DOI: 10.1002/nme

Table II. A measure of the computational cost of the proposed analytical integrations.

	$\mathbf{G}_{uu}$	$\mathbf{G}_{up}$	$\mathbf{G}_{pu}$	$\mathbf{G}_{pp}$
$\mu(\mathbf{G}_{rs})$	10.68	15.79	17.78	9.69

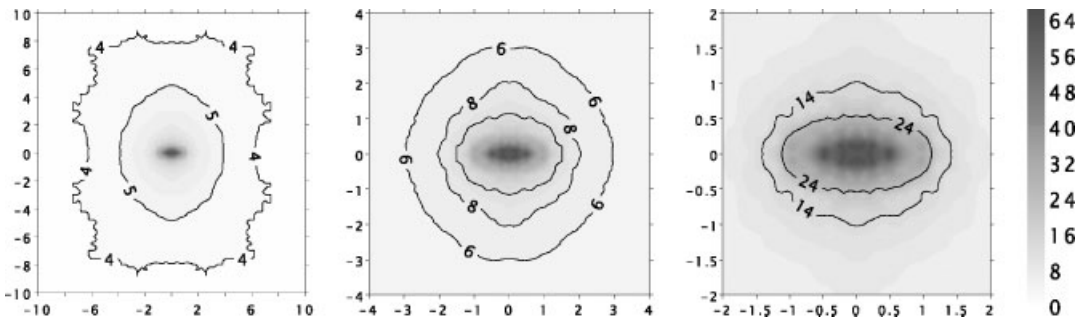

Figure 10. Number of nodes $n_{\text{Gauss}}(\mathbf{x})$ required to reach accuracy ζ for a Gauss quadrature rule about kernel $\mathbf{G}_{uu}$. With reference to Table II the surrounding field is roughly an ellipse with semi-axis $a = 1.75$, $b = 1.5$.

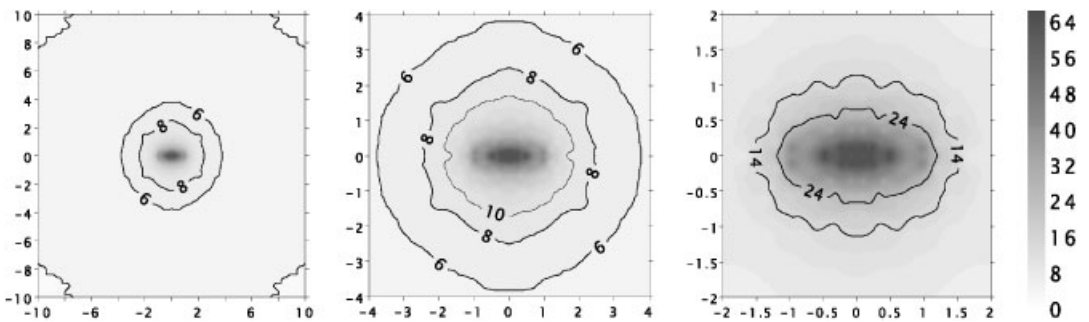

Figure 11. Number of nodes $n_{\text{Gauss}}(\mathbf{x})$ required to reach accuracy ζ for a Gauss quadrature rule about kernel $\mathbf{G}_{up}$. With reference to Table II the surrounding field is roughly an ellipse with semi-axis $a = 1.5$, $b = 1$.

to the field point $\mathbf{x}$ for all four kernels, at three magnifications around the origin. The panel T_{tip} of integral (43) is assumed to coincide with segment $[-1, 1]$ corresponding to a unit half-length l. With reference to Table II, Figures 10–13 highlights three different regions around the panel, a *far* field, a *near* field, and a *surrounding* field. In terms of efficiency, seems devisable the application of fast integral operators in the far field, of numerical quadrature rules in the near-field, and of analytical integrations in the surrounding field. The present analysis stimulated additional work to set up the geometry of the involved regions, even taking into account the several quadrature rules available in the literature: this will be the subject of further study and publications.

DOI: 10.1002/nme

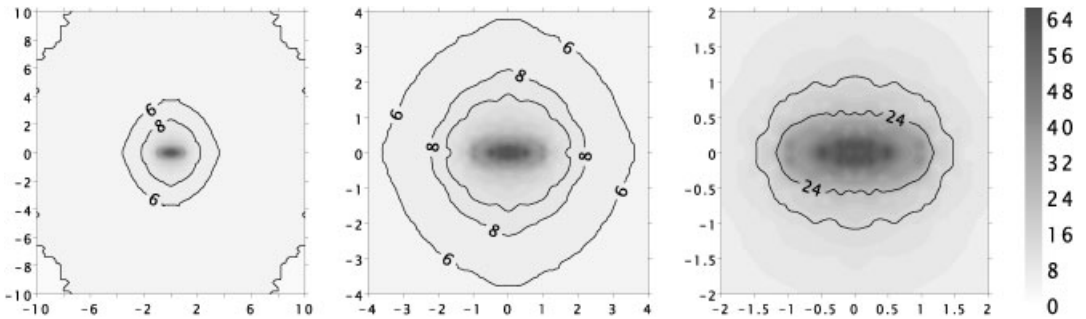

Figure 12. Number of nodes $n_{\text{Gauss}}(\mathbf{x})$ required to reach accuracy ζ for a Gauss quadrature rule about kernel $\mathbf{G}_{pu}$. With reference to Table II the surrounding field is roughly an ellipse with semi-axis $a = 1.3$, $b = 0.8$.

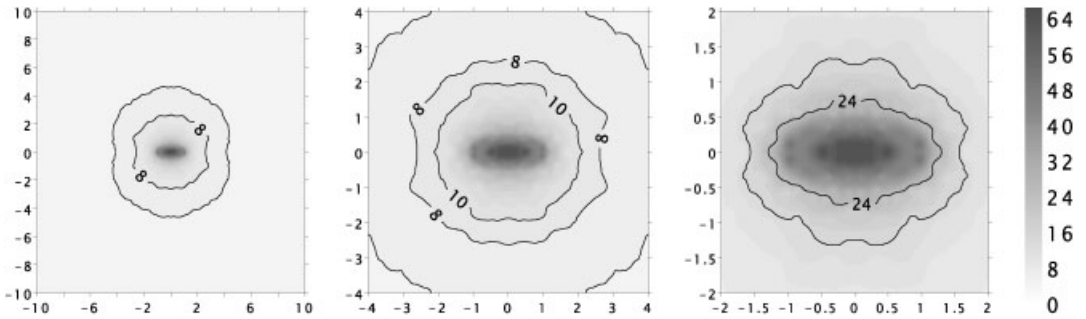

Figure 13. Number of nodes $n_{\text{Gauss}}(\mathbf{x})$ required to reach accuracy ζ for a Gauss quadrature rule about kernel $\mathbf{G}_{pp}$. With reference to Table II the surrounding field is roughly a circle of radius $r = 2$.

5. ANALYTICAL INTEGRATIONS FOR THE GALERKIN SCHEME

5.1. Outer integration singularity analysis

In view of the singular behaviour of function $\mathbf{K}_{pp}(\mathbf{x}, T_{\text{tip}})$ with respect to variable $\mathbf{x}$ in outcome (45), it may be questionable if integrals (14) for SGBEM are of Lebesgue kind even for the hypersingular kernel in the presence of the modified quarter point shape functions (Equation (35)), here rewritten for the sake of clarity:

$$\tilde{\varphi}_j(\xi) = \sum_{i=1}^{4} a_{ij}(l - \xi)^{i/2}, \quad j = 0, 1, 2, \quad a_{2j} = 0 \quad \forall j \tag{67}$$

With the same notation of Section 4.1, define:

$$\mathbf{F}_{pp}(\mathbf{x}, \psi_h) \stackrel{\text{def}}{=} \oint\!\!\!\!\!\!-_{\Gamma_w} \mathbf{G}_{pp}(\mathbf{x} - \mathbf{y}, \mathbf{n}(\mathbf{x}), \mathbf{l}(\mathbf{y}))\psi_h(\mathbf{y})\, \mathrm{d}\Gamma(\mathbf{y})\mathbb{1} \tag{68}$$

DOI: 10.1002/nme

The following proposition holds:

Proposition 5.1
Define shape functions $\psi_k(\mathbf{x})$ and $\psi_h(\mathbf{y})$ as in Equations (27) and (67). Integral

$$\int_{\Gamma_w} \psi_k(\mathbf{x}) \mathbb{1} \ \mathbf{F}_{pp}(\mathbf{x}, \psi_h)\, \mathrm{d}\Gamma(\mathbf{x}) \tag{69}$$

is of Lebesgue-kind.

Proof
Exploiting a result of [6, paragraph 4, p. 1707], the proposition is proved if and only if the singular term in the outer integral for $\mathbf{x} \in T_{\text{tip}}$ and $\mathbf{n}(\mathbf{x}) = \mathbf{e}_2$ reads:

$$-\frac{G}{2\pi}\frac{1}{1-\nu}\int_{T_{\text{tip}}} \psi_k(\mathbf{x})\frac{1}{x_1 + l}\, \mathrm{d}x_1 \mathbb{1} \tag{70}$$

when the inner integral is made over T_{tip}. By shape functions definition (27), the complete form of the inner hypersingular integral—see also Equation (36)—reads:

$$\int_{\Gamma_w} \mathbf{G}_{pp}(\mathbf{r}, \mathbf{n}(\mathbf{x}), \mathbf{l}(\mathbf{y}))\psi_h(\mathbf{y})\, \mathrm{d}\Gamma(\mathbf{y}) = \sum_{T \in \mathscr{T}_h} \int_T \mathbf{G}_{pp}(\mathbf{r}, \mathbf{n}(\mathbf{x}), \mathbf{l}(\mathbf{y}(\xi_1)))\tilde{\varphi}_j(\xi_1)\, \mathrm{d}\xi_1$$

and the term relevant to $T = T_{\text{tip}}$, from Equation (37), splits in the sum:

$$\begin{aligned} &\int_{T_{\text{tip}}} \mathbf{G}_{pp}(\mathbf{x} - \mathbf{y}(\xi_1), \mathbf{n}(\mathbf{x}), \mathbf{l}(\mathbf{y}(\xi_1)))\tilde{\varphi}_0^{\surd}(\xi_1)\, \mathrm{d}\xi_1 \\ &\quad + \int_{T_{\text{tip}}} \mathbf{G}_{pp}(\mathbf{x} - \mathbf{y}(\xi_1), \mathbf{n}(\mathbf{x}), \mathbf{l}(\mathbf{y}(\xi_1)))a_{40}(l - \xi_1)^2\, \mathrm{d}\xi_1 \end{aligned} \tag{71}$$

Assuming $\mathbf{x} \in T_{\text{tip}}$ and $\mathbf{n}(\mathbf{x}) = \mathbf{e}_2$, the first integral in (71) was carried out in Equation (55) and here reprinted for clarity:

$$\frac{G}{2\pi}\frac{1}{1-\nu}\mathbf{r}_{pp}^{\mathsf{T}}(\mathbf{x})\mathbf{X}\mathbf{a}_0 \mathbb{1} \tag{72}$$

where:

$$\begin{aligned} \mathbf{r}_{pp}^{\mathsf{T}}(\mathbf{x}) &= \left[-\frac{\sqrt{d_1}}{d_1}\operatorname{arctanh}\left(\frac{\alpha}{\sqrt{d_1}}\right) - \frac{\alpha}{r_1}, -2\sqrt{d_1}\operatorname{arctanh}\left(\frac{\alpha}{\sqrt{d_1}}\right) + 2\alpha \right]_{r_1=\eta_1-l}^{r_1=\eta_1+l} \\ \mathbf{X} &= \begin{bmatrix} 1 & d_1 \\ 0 & 1 \end{bmatrix}, \quad \mathbf{a}_0 = \begin{bmatrix} a_{10} \\ a_{30} \end{bmatrix} \end{aligned} \tag{73}$$

having set $d_1 = l - \eta_1$, $\alpha = \sqrt{d_1 + r_1}$ with functions $\sqrt{\cdot} : \mathbb{R} \to \mathbb{C}$ and $\operatorname{arctanh}(\cdot) : \mathbb{C} \to \mathbb{C}$. Under the same assumption, the second integral in (71) was carried out in [6], Equation (22), and has

DOI: 10.1002/nme

the same expression of Equation (72) with:

$$\mathbf{r}_{pp}^{\mathsf{T}}(\mathbf{x}) = \left[-\frac{1}{r_1}; \log|r_1|; r_1 \right]_{r_1=\eta_1-l}^{r_1=\eta_1+l}, \quad \mathbf{X} = \begin{bmatrix} 0 & 0 & d_1^2 \\ 0 & 0 & 2d_1 \\ 0 & 0 & 1 \end{bmatrix}, \quad \mathbf{a}_0 = \begin{bmatrix} 0 \\ 0 \\ a_{40} \end{bmatrix} \tag{74}$$

From definitions (73), (74) it comes out that all terms in (72) are Lebesgue integrable with respect to η_1, except:

$$\mathbf{r}_{pp}^{\mathsf{T}}(\mathbf{x})(\mathbf{e}_1 \otimes \mathbf{e}_1)\mathbf{X}\mathbf{a}_0$$

Noting that in Equation (73):

$$\mathbf{r}_{pp}^{\mathsf{T}}(\mathbf{x})\mathbf{e}_1 = -\frac{\sqrt{d_1}}{d_1}\operatorname{arctanh}\left(\frac{\alpha}{\sqrt{d_1}}\right) - \frac{\alpha}{r_1}\Big|_{r_1=\eta_1-l}^{r_1=\eta_1+l} \sim -\frac{\sqrt{2l}}{\eta_1+l} + o\left(\frac{1}{\eta_1+l}\right) \quad \text{for } \eta_1 + l \to 0$$

$$\mathbf{e}_1^{\mathsf{T}}\mathbf{X}\mathbf{a}_0 = \frac{1}{\sqrt{l-\eta_1}}\tilde{\varphi}_0^{\surd}(\eta_1) \sim \frac{1}{\sqrt{2l}}\tilde{\varphi}_0^{\surd}(-l) + o\left(\frac{1}{\eta_1+l}\right) \quad \text{for } \eta_1 + l \to 0$$

and in Equation (74):

$$\mathbf{r}_{pp}^{\mathsf{T}}(\mathbf{x})\mathbf{e}_1 = -\frac{1}{r_1}\Big|_{r_1=\eta_1-l}^{r_1=\eta_1+l} \sim -\frac{1}{\eta_1+l} + o\left(\frac{1}{\eta_1+l}\right) \quad \text{for } \eta_1 + l \to 0$$

$$\mathbf{e}_1^{\mathsf{T}}\mathbf{X}\mathbf{a}_0 = a_{40}(l-\eta_1)^2 \sim 4l^2 a_{40} \quad \text{for } \eta_1 + l \to 0$$

it comes out that the term in (72) non-Lebesgue integrable with respect to η_1 is the following:

$$\frac{G}{2\pi}\frac{\mathbf{r}_{pp}^{\mathsf{T}}(\mathbf{x})(\mathbf{e}_1 \otimes \mathbf{e}_1)\mathbf{X}\mathbf{a}_0}{1-\nu}\mathbb{1} = -\frac{G}{2\pi}\frac{1}{1-\nu}\frac{1}{\eta_1+l}[\tilde{\varphi}_0^{\surd}(-l) + 4l^2 a_{40}]\mathbb{1} = -\frac{G}{2\pi}\frac{1}{1-\nu}\frac{\tilde{\varphi}_0(-l)}{\eta_1+l}\mathbb{1}$$

which, by comparison with (70), proves the theorem.

As outlined in [6, paragraph 4], as well as in Proposition 5.1, Lebesgue nature of integral (69) is due to the mutual cancellation of *all* singularities within 'inner integral' (68). With the notation of (27) and (67), the proof of proposition (5.1) also proves the following corollary:

Proposition 5.2
The following chain of identities holds:

$$\int_{\Gamma_w} \psi_k(\mathbf{x})\mathbb{1}\mathbf{F}_{pp}(\mathbf{x}, \psi_h)\,\mathrm{d}\Gamma(\mathbf{x})$$

$$= \int_{\Gamma_w} \psi_k(\mathbf{x})\mathbb{1} \sum_{T_h \in \mathscr{T}_h} \fint_{T_h} \mathbf{G}_{pp}(\mathbf{x} - \mathbf{y}(\xi), \mathbf{n}(\mathbf{x}), \mathbf{l}(\mathbf{y}(\xi)))\tilde{\varphi}_n(\xi)\mathbb{1}\,\mathrm{d}\xi\,\mathrm{d}\Gamma(\mathbf{x})$$

DOI: 10.1002/nme

$$= \sum_{T_h \in \mathscr{T}_h} \oint\!\!\!\!\!\!- _{\Gamma_w} \psi_k(\mathbf{x}) \mathbb{1} \oint\!\!\!\!\!\!- _{T_h} \mathbf{G}_{pp}(\mathbf{x} - \mathbf{y}(\xi), \mathbf{n}(\mathbf{x}), \mathbf{l}(\mathbf{y}(\xi))) \tilde{\varphi}_n(\xi) \mathbb{1} \, \mathrm{d}\xi \, \mathrm{d}\Gamma(\mathbf{x})$$

$$= \sum_{T_k \in \mathscr{T}_k} \sum_{T_h \in \mathscr{T}_h} \mathbb{1} \oint\!\!\!\!\!\!- _{T_k} \tilde{\varphi}_m(\eta) \oint\!\!\!\!\!\!- _{T_h} \mathbf{G}_{pp}(\mathbf{x}(\eta) - \mathbf{y}(\xi), \mathbf{n}(\mathbf{x}(\eta)), \mathbf{l}(\mathbf{y}(\xi))) \tilde{\varphi}_n(\xi) \, \mathrm{d}\xi \, \mathrm{d}\eta \mathbb{1} \tag{75}$$

5.2. Analytical integration on two equal panels

Consider the factor of integral (75) over crack tip panel $T_k = T_h = T_{\text{tip}}$, equipped with definition (35) of shape functions at T_{tip}, namely:

$$\oint\!\!\!\!\!\!- _{T_{\text{tip}}} \tilde{\varphi}_m(\eta) \oint\!\!\!\!\!\!- _{T_{\text{tip}}} \mathbf{G}_{pp}(\mathbf{r}, \mathbf{n}(\mathbf{x}(\eta)), \mathbf{l}(\mathbf{y}(\xi))) \tilde{\varphi}_n(\xi) \, \mathrm{d}\xi \, \mathrm{d}\eta \tag{76}$$

The inner integral in (76) splits accordingly with (37) in the sum:

$$\oint\!\!\!\!\!\!- _{-l}^{l} \mathbf{G}_{pp}(\mathbf{r}, \mathbf{n}(\mathbf{x}(\eta)), \mathbf{e}_2) \tilde{\varphi}_n^{\surd}(\xi) \, \mathrm{d}\xi + \oint\!\!\!\!\!\!- _{-l}^{l} \mathbf{G}_{pp}(\mathbf{r}, \mathbf{n}(\mathbf{x}(\eta)), \mathbf{e}_2) a_{4n} (l - \xi)^2 \, \mathrm{d}\xi \tag{77}$$

where l is half the length of crack tip panel T_{tip}. For being $\mathbf{x} \in T_{\text{tip}}$ too, $-l \leqslant \eta \leqslant l$ and $\mathbf{n}(\mathbf{x}) = \mathbf{e}_2$, the first integral in (77) becomes alike the one carried out in Equation (61), reprinted here:

$$\oint\!\!\!\!\!\!- _{-l}^{l} \mathbf{G}_{pp}(\mathbf{r}, \mathbf{e}_2, \mathbf{e}_2) \tilde{\varphi}_n^{\surd}(\xi) \, \mathrm{d}\xi \Big|_{\mathbf{x} \in T_{\text{tip}}}$$

$$= \frac{G}{16\pi(1-\nu)} \times \left\{ -4\sqrt{|\mathbf{d}|} \log \frac{\sqrt{|\mathbf{d}|} + \sqrt{2l}}{|\sqrt{|\mathbf{d}|} - \sqrt{2l}|} \left\{ \frac{1}{|\mathbf{d}|}, 2 \right\} \right.$$

$$\left. + \; 16\sqrt{2l}\{0, 1\} - 8\frac{\sqrt{2l}}{\eta + l}\{1, 0\} \right\} \mathbf{X}\mathbf{a}_n \mathbb{1} \tag{78}$$

denoting with $d_1 = l - \eta$ and vector $\mathbf{d}$ such that $0 \leqslant |\mathbf{d}| = d_1 \leqslant 2l$. Matrix $\mathbf{X}$ and vector $\mathbf{a}_n$ have been defined by formula (41):

$$\mathbf{X}\mathbf{a}_n = \begin{bmatrix} a_{1n} + d_1 a_{3n} \\ a_{3n} \end{bmatrix}$$

As already shown in the proof of Proposition 5.1, the last factor in double brackets in identity (78) produces a non-integrable singularity for the outer integral, which reads:

$$-8\frac{\sqrt{2l}}{\eta + l}\{1, 0\}\mathbf{X}\mathbf{a}_n|_{\eta = -l} = -8\frac{\sqrt{2l}}{\eta + l}(a_{1n} + 2l a_{3n})$$

Noting that

$$\{1, 0\}\mathbf{X}\mathbf{a}_n - \{1, 0\}\mathbf{X}\mathbf{a}_n|_{\eta = -l} = -a_{3n}(\eta + l)$$

DOI: 10.1002/nme

it comes out straightforwardly:

$$\begin{aligned}&\oint_{-l}^{l}\tilde{\varphi}_m(\eta)\oint_{-l}^{l}\mathbf{G}_{pp}(\mathbf{r},\mathbf{e}_2,\mathbf{e}_2)\tilde{\varphi}_n^{\surd}(\xi)\,\mathrm{d}\xi\,\mathrm{d}\eta\\&=\frac{G}{16\pi(1-\nu)}\oint_{0}^{2l}\tilde{\varphi}_m(d_1)\left\{-4\sqrt{d_1}\log\frac{\sqrt{2l}+\sqrt{d_1}}{\sqrt{2l}-\sqrt{d_1}}\left(\frac{a_{1n}}{d_1}+3a_{3n}\right)+24\sqrt{2l}a_{3n}\right\}\mathrm{d}d_1\,\mathbb{1}\end{aligned}\tag{79}$$

The second integral in (77) was carried out in [6], Equation (22):

$$\oint_{-l}^{l}\mathbf{G}_{pp}(\mathbf{r},\mathbf{e}_2,\mathbf{e}_2)a_{4n}(l-\xi)^2\,\mathrm{d}\xi=\frac{G}{2\pi}\frac{a_{4n}}{1-\nu}\left\{-\frac{d_1^2}{r_1}+2d_1\log|r_1|+r_1\right\}_{r_1=\eta-l}^{r_1=\eta+l}\mathbb{1}\tag{80}$$

The first factor in double brackets in identity (80) produces a non-integrable singularity for the outer integral, which reads:

$$-\frac{G}{2\pi}\frac{a_{4n}}{1-\nu}\frac{(2l)^2}{\eta+l}\mathbb{1}$$

Noting that

$$d_1^2-(2l)^2=(\eta-3l)(\eta+l)$$

it comes out straightforwardly:

$$\begin{aligned}&\oint_{-l}^{l}\tilde{\varphi}_m(\eta)\oint_{-l}^{l}\mathbf{G}_{pp}(\mathbf{r},\mathbf{e}_2,\mathbf{e}_2)a_{4n}(l-\xi)^2\,\mathrm{d}\xi\,\mathrm{d}\eta\\&=\frac{Ga_{4n}}{2\pi(1-\nu)}\oint_{-l}^{l}\tilde{\varphi}_m(\eta)\left\{2(l-\eta)\log\frac{l+\eta}{l-\eta}+4l\right\}\mathrm{d}\eta\mathbb{1}\end{aligned}\tag{81}$$

In view of splitting (77), integral (76) is the sum of (79) and (81): it reads

$$\oint_{T_{\mathrm{tip}}}\tilde{\varphi}_m(\eta)\oint_{T_{\mathrm{tip}}}\mathbf{G}_{pp}(\mathbf{r},\mathbf{n}(\mathbf{x}(\eta)),\mathbf{l}(\mathbf{y}(\xi)))\tilde{\varphi}_n(\xi)\,\mathrm{d}\xi\,\mathrm{d}\eta=\frac{Gl}{105\pi(1-\nu)}\sum_{i=0}^{6}\kappa_{i/2}l^{i/2}\mathbb{1}\tag{82}$$

where κ_j are coefficients that merely depend upon shape functions $\tilde{\varphi}_m$, $\tilde{\varphi}_n$ as defined in (67) and read as follows:

$$\begin{aligned}\kappa_0&=-105\,a_{1m}\,a_{1n}\\\kappa_{1/2}&=0\\\kappa_1&=-140\,a_{1n}\,a_{3m}\\\kappa_{3/2}&=21\sqrt{2}[8a_{1m}a_{4n}(-1+\log 4)-a_{1n}a_{4m}(3+\log 16)]\\\kappa_2&=-140a_{3m}a_{3n}\\\kappa_{5/2}&=10\sqrt{2}[9a_{3n}(1-4\log 2)a_{4m}+8a_{3m}a_{4n}(-5+\log 64)]\\\kappa_3&=-210a_{4m}a_{4n}\end{aligned}\tag{83}$$

DOI: 10.1002/nme

6. ASYMPTOTICAL ANALYSIS AND SIF EVALUATION

Further to the numerical approximation of problem (10), several methods [49] allow for the evaluation of SIFs, deducing them from related quantities (J or M-integrals [25, 50]) or from asymptotic relationships that hold for the exact solution (one or two point displacement correlation techniques [51], traction correlation technique [52]). By exploiting analytical integrations of Section 4, a direct and coherent approximation of SIFs can be obtained by the asymptotic analysis of representation formula (6) by means of the evaluated numerical approximation y_h. By neglecting volume forces, BIR (6) becomes:

$$\mathbf{p}_h(\mathbf{x},\mathbf{n}(\mathbf{x}))+\int_{\Gamma_p}\mathbf{G}_{pp}(\mathbf{r};\mathbf{n}(\mathbf{x});\mathbf{l}(\mathbf{y}))\mathbf{u}_h(\mathbf{y})\mathrm{d}\mathbf{y}+\int_{\Gamma_u}\mathbf{G}_{pp}(\mathbf{r};\mathbf{n}(\mathbf{x});\mathbf{l}(\mathbf{y}))\bar{\mathbf{u}}(\mathbf{y})\,\mathrm{d}\mathbf{y}$$

$$+\int_{\Gamma_w}\mathbf{G}_{pp}(\mathbf{r};\mathbf{n}(\mathbf{x});\mathbf{l}(\mathbf{y}))\mathbf{w}_h(\mathbf{y})\,\mathrm{d}\mathbf{y}=\int_{\Gamma_u}\mathbf{G}_{pu}(\mathbf{r};\mathbf{n}(\mathbf{x}))\mathbf{p}_h(\mathbf{y})\,\mathrm{d}\mathbf{y}$$

$$+\int_{\Gamma_p}\mathbf{G}_{pu}(\mathbf{r};\mathbf{n}(\mathbf{x}))\bar{\mathbf{p}}(\mathbf{y})\,\mathrm{d}\mathbf{y},\quad \mathbf{x}\in\Omega \tag{84}$$

If the field point $\mathbf{x}$ is assumed to coincide with the crack tip, contributions of integrals over Γ_u and of Γ_p are finite quantities that, in view of the singularity of the stress field, plays a minor role; the same statement applies to all boundary elements on Γ_w not enclosing the crack tip. Accordingly, a ball $\mathscr{B}^{\delta}_{\mathrm{tip}}$ of radius δ centred at the crack tip can be considered such that for all points $\mathbf{x}\in\mathscr{B}^{\delta}_{\mathrm{tip}}$:

$$\mathbf{p}_h(\mathbf{x},\mathbf{n}(\mathbf{x}))+\int_{T_{\mathrm{tip}}}\mathbf{G}_{pp}(\mathbf{r};\mathbf{n}(\mathbf{x});\mathbf{l}(\mathbf{y}))\mathbf{w}_h(\mathbf{y})\,\mathrm{d}\mathbf{y}=O(1),\quad \mathbf{x}\in\mathscr{B}^{\delta}_{\mathrm{tip}} \tag{85}$$

Owing to Equations (35) and (37), the approximation for $\mathbf{p}_h(\mathbf{x},\mathbf{n}(\mathbf{x}))$ reads:

$$\mathbf{p}_h(\mathbf{x},\mathbf{n}(\mathbf{x}))=-\sum_{j=0}^{2}\int_{-l}^{l}\mathbf{G}_{pp}(\mathbf{x}-\mathbf{y}(\xi);\mathbf{n}(\mathbf{x});\mathbf{l}(\mathbf{y}(\xi)))\tilde{\varphi}_j^{\surd}(\xi)\,\mathrm{d}\xi\,\mathbf{w}_j$$

$$-\sum_{j=0}^{2}\int_{-l}^{l}\mathbf{G}_{pp}(\mathbf{x}-\mathbf{y}(\xi);\mathbf{n}(\mathbf{x});\mathbf{l}(\mathbf{y}(\xi)))[a_{4j}(l-\xi)^2]\,\mathrm{d}\xi\,\mathbf{w}_j+O(1),\quad \mathbf{x}\in\mathscr{B}^{\delta}_{\mathrm{tip}} \tag{86}$$

In view of outcomes published in [6], the second integral in Equation (86) vanishes when $\delta\to 0$; from Equation (40), with notation of Figure 7 and normal $\mathbf{l}(\mathbf{y}(\xi))=-\mathbf{e}_2$ by definition of normal at a crack—see Figure 1, it comes out:

$$\mathbf{p}_h(\mathbf{x},\mathbf{n}(\mathbf{x}))=-\sum_{j=0}^{2}\int_{-d_1}^{2l-d_1}\mathbf{G}_{pp}(\mathbf{r};\mathbf{n}(\mathbf{x});-\mathbf{e}_2)\mathbf{r}_1^{\mathsf{T}}\sqrt{d_1+r_1}\,\mathrm{d}r_1\Big|_{r_2=-d_2}$$

$$\times\mathbf{X}\mathbf{a}_j\mathbf{w}_j+O(1),\quad \mathbf{x}\in\mathscr{B}^{\delta}_{\mathrm{tip}} \tag{87}$$

DOI: 10.1002/nme

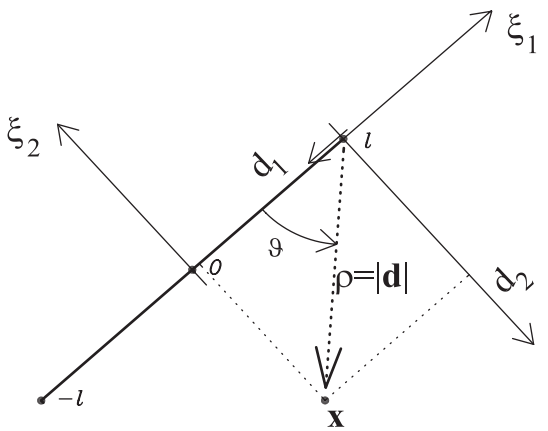

Figure 14. Polar co-ordinate system.

By a polar reference change $d_1 = \rho \cos \vartheta$, $d_2 = \rho \sin \vartheta$–see Figure 14—and in view of identity (45), integral (87) can be written in the form:

$$\mathbf{p}_h(\mathbf{x}, \mathbf{n}(\mathbf{x})) = \frac{\mathbf{k}(\vartheta)}{\sqrt{\rho}} + O(1), \quad \mathbf{x} \in \mathscr{B}^{\delta}_{\text{tip}} \tag{88}$$

which seems to be a relevant property of integral operator $\int_{\Gamma_w} \mathbf{G}_{pp}(\mathbf{r}; \mathbf{n}(\mathbf{x}); \mathbf{l}(\mathbf{y})) \cdot \mathrm{d}\mathbf{y}$ and can be stated as follows:

Proposition 6.1
Denote with $\mathbf{e}_1 = \{1, 0\}$ the usual unit vector. Define $\boldsymbol{\eta} = \{\eta_1, \eta_2\}$, $\vartheta = \arctan \eta_2/(\eta_1 - l)$, $\boldsymbol{\xi} = \{\xi_1, 0\}$. Define the ball $\mathscr{B}^{\delta}_{\text{tip}}$ as the set:

$$\mathscr{B}^{\delta}_{\text{tip}} = \{\boldsymbol{\eta} \in \mathbb{R}^2 \text{ s.t. } \|\boldsymbol{\eta} - l\mathbf{e}_1\| < \delta\}$$

It exists a vector valued function $\mathbf{k} : \mathbb{R} \to \mathbb{R}^2$ such that $\forall \varepsilon > 0$, $\exists \delta > 0$ s.t. $\forall \boldsymbol{\eta} \in \mathscr{B}^{\delta}_{\text{tip}}$:

$$\left| \sqrt{\|\boldsymbol{\eta} - l\mathbf{e}_1\|} \int_{-l}^{l} \mathbf{G}_{pp}(\boldsymbol{\eta} - \boldsymbol{\xi}; \mathbf{n}(\boldsymbol{\eta}), -\mathbf{e}_2) \sqrt{l - \xi_1}\, \mathrm{d}\xi_1 - \mathbf{k}(\vartheta) \right| < \varepsilon$$

Proposition 6.1 motivates the use of $\sqrt{\rho}$-type shape functions (as quarter point and their enhancements) in the context of BIEs, insuring the capability of the approximated traction field $\mathbf{p}_h(\mathbf{x}, \mathbf{n}(\mathbf{x}))$ to reproduce the asymptotic behaviour of the exact solution around the crack tip**** inside the domain $\Omega \cap \mathscr{B}^{\delta}_{\text{tip}}$.

****Differently from the finite element scheme, in BIEs the shape functions are merely defined along the boundary $\partial\Omega$ and can model the approximated field in the domain Ω only through the application of operator $\mathscr{L}$ of Equation (10).

DOI: 10.1002/nme

Proposition 6.2
It comes out[††††] at $\vartheta = \pi$:

$$\mathbf{p}_h(\{\rho, \pi\}, \mathbf{n}(\{\rho, \pi\})) = \frac{G}{4\,(1-\nu)} \begin{bmatrix} n_2 & n_1 \\ n_1 & n_2 \end{bmatrix} \frac{1}{\sqrt{\rho}} \frac{\sqrt{2}}{11\sqrt{l}} \left(\mathbf{w}_0 - \frac{27}{4}\mathbf{w}_1 + 27\mathbf{w}_2 \right) \tag{89}$$

Equation (89) seems to be of practical interest. It is well known from Westergaard's asymptotic analysis [45] that for $\mathbf{x}$ in front of the crack tip, i.e. at $\vartheta = \pi$ with notation of Figure 14, the SIF vector holds:

$$\mathbf{K} = \begin{bmatrix} K_{\mathrm{I}} \\ K_{\mathrm{II}} \end{bmatrix} = \lim_{\rho \to 0} \sqrt{2\pi\rho}\mathbf{p}(\{\rho, \pi\}, \mathbf{e}_1)$$

Equation (89) furnishes a direct approximation $\mathbf{K}_h$ of the SIF vector, being:

$$\mathbf{K}_h = \frac{G}{4\,(1-\nu)} \begin{bmatrix} 0 & 1 \\ 1 & 0 \end{bmatrix} \frac{2\sqrt{\pi}}{11\sqrt{l}} \left(\mathbf{w}_0 - \frac{27}{4}\mathbf{w}_1 + 27\mathbf{w}_2 \right) \tag{90}$$

Formula (90) is *coherent with the approximation* y_h, in the sense that it gives the value of SIFs corresponding to the approximated stress field in domain Ω. Other approaches for SIFs approximation—e.g. the J-integral [50] or the one point formula [4]—do not possess this property. An approach similar to formula (90) has been pursued in the literature, approximating SIFs via a least squares fitting of stress tensors numerically evaluated at a cloud of points close to the crack tip.

Formula (90) can be obtained also by a different approach. Stemming from the identity [31]:

$$\mathbf{K} = \frac{G}{4(1-\nu)} \lim_{\rho \to 0} \sqrt{\frac{2\pi}{\rho}} \begin{bmatrix} 0 & 1 \\ 1 & 0 \end{bmatrix} \mathbf{w}(\rho, \vartheta = 0) \tag{91}$$

assume for $\mathbf{w}(\rho, \vartheta = 0)$ approximation (35) with $\tilde{\varphi}_j(\xi)$ as in Appendix A. It is straightforward proving that

$$\begin{aligned} &\frac{G}{4\,(1-\nu)} \lim_{\rho \to 0} \sqrt{\frac{2\pi}{\rho}} \begin{bmatrix} 0 & 1 \\ 1 & 0 \end{bmatrix} \sum_{j=0}^{2} \mathbf{w}_j \tilde{\varphi}_j(\xi) \\ &\quad = \frac{G}{4(1-\nu)} \begin{bmatrix} 0 & 1 \\ 1 & 0 \end{bmatrix} \frac{2\sqrt{\pi}}{11\sqrt{l}} \left(\mathbf{w}_0 - \frac{27}{4}\mathbf{w}_1 + 27\mathbf{w}_2 \right) \end{aligned} \tag{92}$$

that is, Equation (90). The equivalence of the two approaches seems to be significant: Equation (90) is the outcome of an asymptotic analysis of the stress field after the discretization whereas Equation (91) comes out from William's asymptotic analysis of the displacement field near the crack tip apart of any discretization process. The equivalence property is inherited from the use

[††††]For the 2D plane stress case, ν must be replaced by $\nu^* = \nu/(1+\nu)$.

DOI: 10.1002/nme

of an exact BIR formula and of the analytical integrations and is therefore a property of the BEM (it does not apply for different computational techniques) in the presence of analytical integrations.

The latter approach is well known [31] to derive the so-called 'two-point formula' once applied to the standard quarter point (QP) element. As the QP shape functions are a special case of (35), the stated equivalence seem to reveal that the two-point formula is privileged with respect to all other SIFs approximation formulas in the framework of LEFM via BIEs.

7. NUMERICAL APPROXIMATIONS OF SIFS

Muskhelishvili's problem: Consider an homogeneous, isotropic linear elastic material occupying an unbounded domain $\Omega = \mathbb{R}^2$. Consider a line crack of length 2, whose midpoint coincides with the origin of the co-ordinate system $\{x_1, x_2\}$, slanted by angle θ from x_1 axis as in Figure 15. Assuming that the crack is pressurized by a traction $\bar{\mathbf{p}}_w(\mathbf{x}) = -\bar{p}_w\,(\mathbf{e}_2 \cdot \mathbf{n}(\mathbf{x}))\mathbf{e}_2$, the plane stress solution is given in closed form, see e.g. [53]. SIFs hold:

$$K_{\mathrm{I}} = \bar{p}_w\sqrt{\pi}\,\cos^2(\theta), \quad K_{\mathrm{II}} = \bar{p}_w\sqrt{\pi}\cos(\theta)\sin(\theta) \tag{93}$$

and are independent on the material constitutive parameters. Muskhelishvili's problem has been approximated via the hypersingular collocation BEM by means of 3 uniform meshes (named mesh 1, 2, 3), of panel length $1 = l_1 = 2l_2 = 4l_3$.

The relative error in the approximations of SIFs are collected in Table III for the hypersingular collocation approach, by placing collocation point at the Gauss nodes on the element. The first line (q) refers to quadratic elements without making recourse to any special element at the crack tip. The remaining three sets of analysis concern of quadratic elements using standard quarter point crack tip (sQP), modified QP (mQP) as in [31], enhanced QP (eQP) as in Section 3. Quite unexpectedly, the accuracy shows to be independent on the direction (K_{I} or K_{II}) as well as on the slanted angle θ.

The relative error in the approximations of SIFs for the Galerkin scheme are collected in Table IV. Again, the accuracy shows to be independent on the direction (K_{I} or K_{II}) as well as on the slanted angle θ.

Edge crack: Consider a square plate of width h with a single edge crack of length a, as in Figure 16. The plate is subjected to the action of a uniform unit traction, applied symmetrically

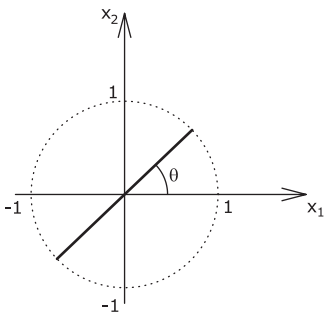

Figure 15. Muskhelishvili's problem.

DOI: 10.1002/nme

Table III. Accuracy (in %) of SIFs approximation of Muskhelishvili's problem for the collocation approach: the accuracy for K_{I} and K_{II} is equal.

		Boundary elements along the crack								
Type	SIF formula	2	4	8	2	4	8	2	4	8
q	one pt	40.87	21.95	14.37	40.87	21.95	14.37	40.87	21.95	14.37
sQP	one pt	1.98	0.17	0.12	1.98	0.17	0.12	1.98	0.17	0.12
	two pts	29.89	12.68	5.68	29.89	12.68	5.68	29.89	12.68	5.68
mQP	one pt	4.85	2.86	1.51	4.85	2.86	1.51	4.85	2.86	1.51
	two pts	2.95	0.56	0.08	2.95	0.56	0.08	2.95	0.56	0.08
eQP	one pt	3.56	1.45	0.64	3.56	1.45	0.64	3.56	1.45	0.64
	(90)	1.40	0.11	0.08	1.40	0.11	0.08	1.40	0.11	0.08
		$\theta=0$			$\theta=\frac{\pi}{6}$			$\theta=\frac{\pi}{3}$		
		Slanted angle θ								

Table IV. Accuracy (in %) of SIFs approximation of Muskhelishvili's problem for the Galerkin approach: the accuracy for K_{I} and K_{II} is equal.

		Boundary elements along the crack								
Type	SIF formula	2	4	8	2	4	8	2	4	8
q	one pt	37.34	18.41	11.22	37.34	18.41	11.22	37.34	18.41	11.22
sQP	one pt	6.43	3.17	1.60	6.43	3.17	1.60	6.43	3.17	1.60
	two pts	14.39	6.55	3.01	14.39	6.55	3.01	14.39	6.55	3.01
mQP	one pt	6.12	3.12	1.58	6.12	3.12	1.58	6.12	3.12	1.58
	two pts	1.44	0.28	0.02	1.44	0.28	0.02	1.44	0.28	0.02
eQP	one pt	2.87	1.38	0.68	2.87	1.38	0.68	2.87	1.38	0.68
	(90)	0.40	0.01	0.04	0.40	0.01	0.04	0.40	0.01	0.04
		$\theta=0$			$\theta=\frac{\pi}{6}$			$\theta=\frac{\pi}{3}$		
		Slanted angle θ								

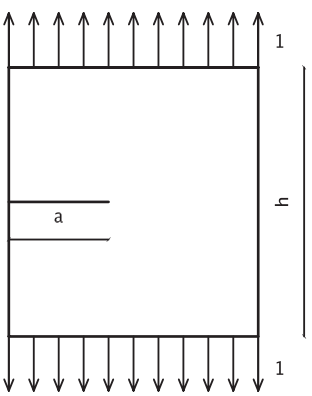

Figure 16. Square plate with a single edge crack.

DOI: 10.1002/nme

Table V. Edge crack K_I approximation.

$\frac{a}{h}$	QP	λ 0.5	1	2	4	Reference [4]
0.25	*s*	—	4.112	4.130	4.134	—
	e	—	4.155	4.153	4.154	
0.5	*s*	8.327	9.445	10.050	10.350	10.670
	e	10.634	10.669	10.675	10.677	
0.75	*s*	23.27	28.99	32.53	34.51	—
	e	38.12	36.91	36.77	36.77	
0.9375	*s*	—	−47.9	395.289	612.82	—
	e	—	1990.8	1135.5	1072.57	

The quarter point (QP) column indicates standard (*s*) versus enhanced (*e*). Results of the analysis at $a/h = 0.5$ can be compared with $K_I = 10.670$ from Table 1 at p. 129 in Reference [4]. Results of the last-row analysis, $a/h = 0.9375$ can be compared with a $K_I = 1017.3$ reference solution obtained by a non-uniform mesh refined around the crack tip.

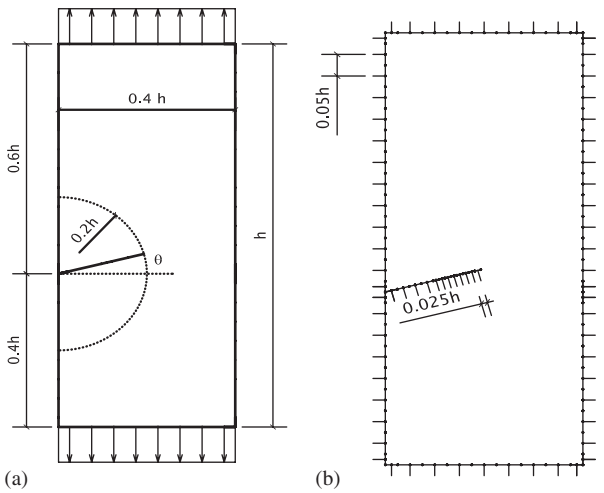

Figure 17. Rectangular plate with a single edge slant crack: (a) the geometry and the unit applied loads; and (b) the discretization, refined at corners and at the crack tip.

at the ends in the direction perpendicular to the crack. The value of K_I is evaluated for several a/h ratios and several uniform meshes, of panel length $l = h/(8\lambda)$ with $\lambda = \frac{1}{4}, \frac{1}{2}, 1, 2$. Results are collected in Table V and are obtained by the Galerkin scheme using the two-point formula for the standard quarter point and formula (90) for the enhanced quarter point elements. K_I values can be compared with results of Table I at p. 129 in Reference [4].

Edge slant crack: Consider a rectangular plate of height h and width $0.4h$—as in Figure 17(a)—with a single left-edge crack of length $0.2h$ starting at a distance $0.4h$ from the bottom side.

DOI: 10.1002/nme

Table VI. Edge slant crack K_{I} and K_{II} approximation.

	CBEM				SGBEM			
θ	K_{I}	K_{II}	$\frac{E\,J}{1-\nu^2}$	ζ (%)	K_{I}	K_{II}	$\frac{E\,J}{1-\nu^2}$	ζ (%)
−85	0.91148	−0.25965	0.87689	2.43	0.49110	−0.57818	0.57619	0.13
−80	0.97428	−0.88712	1.73052	0.33	0.89290	−0.94395	1.68664	0.10
−75	1.39453	−1.28552	3.58633	0.31	1.37308	−1.29769	3.56522	0.12
−70	1.96079	−1.63886	6.51154	0.29	1.95396	−1.64048	6.50173	0.11
−65	2.64237	−1.96244	10.8034	0.28	2.63892	−1.96169	10.8004	0.11
−60	3.42499	−2.25187	16.758	0.26	3.42238	−2.25057	16.761	0.10
−55	4.29874	−2.50052	24.672	0.24	4.29634	−2.49915	24.6822	0.09
−50	5.25636	−2.70205	34.8522	0.22	5.25402	−2.70074	34.872	0.08
−45	6.29066	−2.84712	47.5807	0.21	6.28944	−2.84695	47.6328	0.06
−40	7.39407	−2.92576	63.1154	0.19	7.3934	−2.92559	63.1934	0.04
−35	8.54805	−2.92125	81.4691	0.16	8.54808	−2.92101	81.5814	0.03
−30	9.72156	−2.81718	102.3	0.14	9.7226	−2.81681	102.458	0.01
−25	10.8692	−2.60052	124.752	0.12	10.8716	−2.60001	124.972	0.02
−20	11.9335	−2.26567	147.394	0.10	11.9379	−2.26504	147.692	0.03
−15	12.8509	−1.81721	168.305	0.08	12.8575	−1.81649	168.697	0.05
−10	13.5593	−1.27077	185.332	0.07	13.5682	−1.26998	185.818	0.06
−5	14.0068	−0.65203	196.479	0.07	14.0175	−0.651137	197.038	0.06
0	14.165	—	200.71	0.03	14.17	—	200.93	0.07
5	14.0025	0.66597	196.345	0.09	14.0127	0.66695	196.895	0.05
10	13.5483	1.29129	185.028	0.11	13.5563	1.29204	185.495	0.03
15	12.8283	1.84865	167.757	0.13	12.8336	1.84902	168.121	0.00
20	11.8916	2.31182	146.507	0.17	11.8944	2.31174	146.772	0.03
25	10.7979	2.66342	123.431	0.21	10.7988	2.66295	123.616	0.07
30	9.61014	2.8956	100.487	0.25	9.60977	2.89485	100.614	0.11
35	8.388	3.00937	79.1822	0.29	8.38691	3.00849	79.2693	0.15
40	7.18317	3.01309	60.4746	0.33	7.18174	3.01218	60.5347	0.19
45	6.03657	2.92039	44.8031	0.37	6.03496	2.91951	44.8436	0.22
50	4.97723	2.74852	32.1985	0.40	4.97554	2.74717	32.2222	0.25
55	4.02294	2.51425	22.4107	0.42	4.02129	2.51298	22.4255	0.27
60	3.18219	2.23522	15.0565	0.44	3.18033	2.23411	15.0637	0.28
65	2.45567	1.92639	9.69788	0.45	2.45287	1.92589	9.69849	0.28
70	1.83939	1.59888	5.91309	0.45	1.8331	1.60077	5.9066	0.27
75	1.33142	1.2549	3.33219	0.46	1.31047	1.26734	3.31499	0.26
80	0.95081	0.87131	1.65426	0.54	0.86993	0.92847	1.61535	0.22
85	0.90716	0.25560	0.86398	2.81	0.48685	0.57424	0.56700	0.04

The crack is slanted by angle θ: analysis have been carried out for θ in the range $[-80°, 80°]$. The plate is subjected to the action of a uniform unit traction, applied symmetrically at the two horizontal sides in the direction orthogonal to the boundary.

Analysis have been performed by means of two set of discretizations: for angle $|\theta| \leqslant 45°$, a panel length of $0.05h$ has been considered to produce a uniform mesh of quadratic BEs on the boundary and along the crack. The mesh has been refined in vicinity of the corners as well as of the crack tip (see Figure 17(b)), where the enhanced quarter point crack tip element has been placed. For angle $|\theta| > 45°$ the mesh on the left side of the plate has been refined, by doubling the number of elements.

DOI: 10.1002/nme

Analysis have been preformed for the hypersingular collocation as well as for the symmetric Galerkin schemes: results are collected in Table VI, in terms of K_{I}, K_{II} and the J-integral $EJ/(1-\nu^2)$. In view of the relation

$$\frac{EJ}{1-\nu^2} = K_{\mathrm{I}}^2 + K_{\mathrm{II}}^2$$

the number

$$\zeta = \frac{\left| J - (1-\nu^2)\dfrac{K_{\mathrm{I}}^2 + K_{\mathrm{II}}^2}{E} \right|}{J}$$

can be assumed as a measure of accuracy of the numerical approximation of K_{I}, K_{II} and is also presented in Table VI. Figure 18 plot K_{I} and K_{II} against the slanted angle θ.

A propagating, *pressurized centre crack*: Consider a square plate of side h—as in Figure 19—with a single horizontal central crack of initial length $h/24$. No loads are prescribed along the exterior boundary $\partial\Omega$; the crack propagates under the effect of a normal pressure λ acting on the interval $-h/48 \leqslant x_1 \leqslant h/48$, independent on the actual crack length. The target of the simulation is the approximation of the critical load-factor λ_c and the critical crack length that correspond to λ_c.

Discretization has been performed by means of a quasi-uniform quadratic mesh with panel length of $h/80$ along $\partial\Omega$ and of $h/120$ along the crack. Results, referring to the Galerkin scheme, are plotted in Figure 19. Load factor λ at any given crack length is evaluated such that $K_{\mathrm{I}} = K_{\mathrm{I}c}$: accordingly, the condition of onset of propagation is kept in the load process; values of ratio λ over $K_{\mathrm{I}c}$ are plotted on the vertical axis. The critical load factor, after which a crack advance implies a load decrement (the unstable crack growth region), is reached at $\lambda_c \simeq 1.9 K_{\mathrm{I}c}$ corresponding to a critical crack length of about $0.35h$. It is worth here noting that the unstable crack growth can be simulated because as 'control parameter' has been assumed the actual crack length, which is monotonically increasing. In a general case this approach reveals unsatisfactory and different strategies are recommended for evaluating the safety factor of a cracked structural component.

8. CONCLUDING REMARKS

An accurate evaluation of the structural response of a cracked body to external actions seems to be important to assess safety against failure due to fracture propagation. Notwithstanding unavoidable nonlinear dissipative phenomena—due to plastic deformations around crack tip, or to cohesive forces in the process zone—LEFM is still of primary importance, especially when the size may infer brittleness to a cracked body. In computational LEFM a major task consists in the approximation of SIFs, as they govern propagation and stability of fractures: several methods and *ad hoc* shape functions have been proposed in order to increase accuracy in SIFs evaluation. The present note concerned LEFM problems modelled by means of BIEs (10): analytical integrations have been presented—both as a limit of a Lebesgue integral and directly in a CPV and Hadamard's finite parts sense—in Section 4 for BIR formulae as well as for the collocation scheme. With reference

DOI: 10.1002/nme

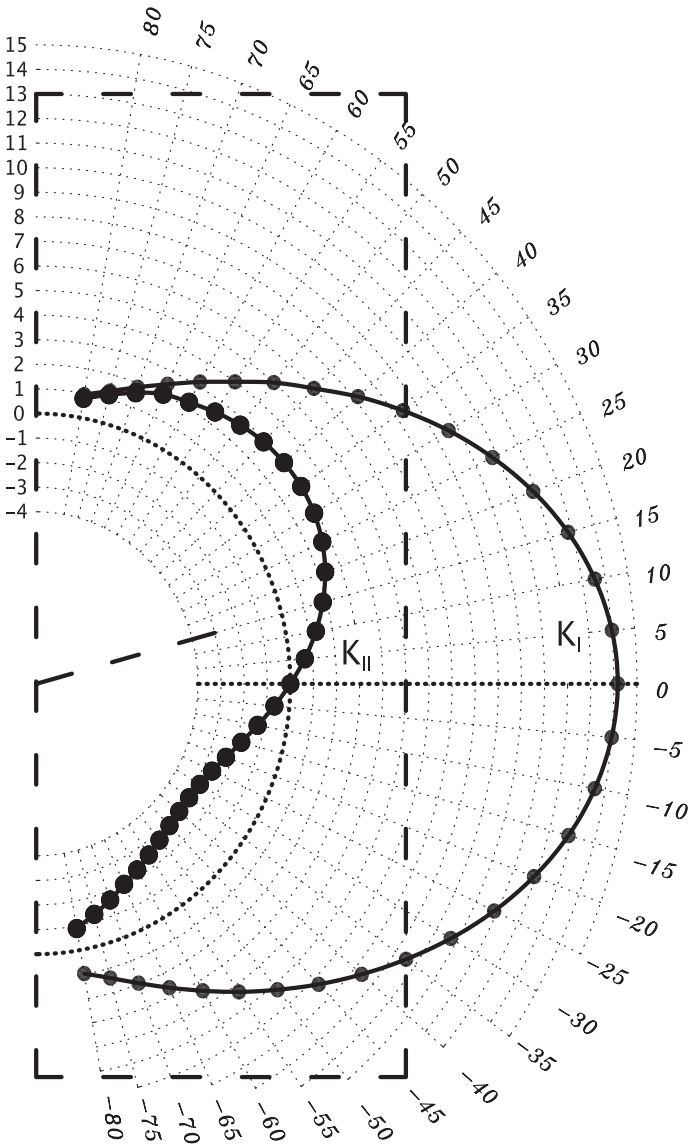

Figure 18. Rectangular plate with a single edge slant crack: SIF approximation.

to the Galerkin method it has been proved in Section 5.1 that the bilinear form for BIEs (Equation (11)) has a Lebesgue nature even in the presence of shape functions (35) that incorporate the square-root behaviour of crack opening displacement.

In definition (35) the crack tip has been assumed to be located at the right-end of an element, that is at $\xi = l$; the same assumption has been considered into the rest of the note. It is straightforward extending the basic results to the case of crack tip at the left-end side at $\xi = -l$.

DOI: 10.1002/nme

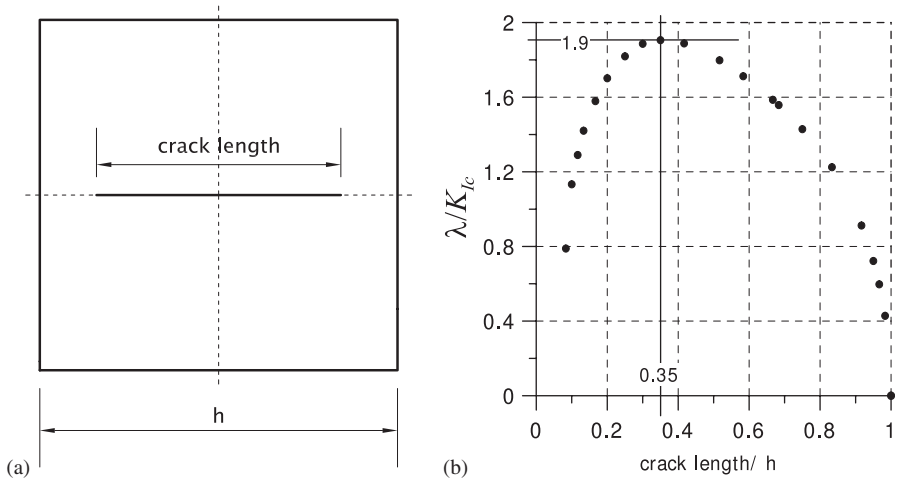

Figure 19. Square plate with a single propagating central crack: (a) geometry; and (b) load versus crack length behaviour.

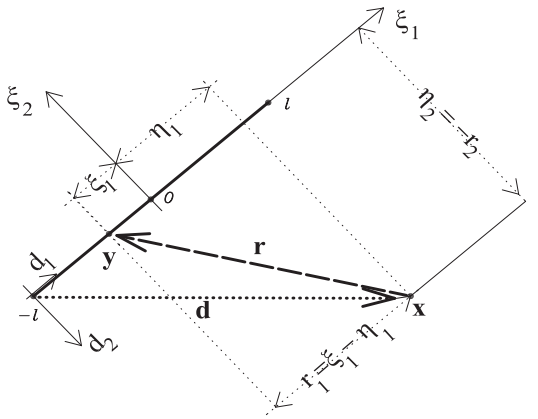

Figure 20. Notation for crack tip at $\xi=-l$.

Identity (35) becomes:

$$\mathbf{w}(\xi)=\sum_{j=0}^{2}\mathbf{w}_j\tilde{\varphi}_j(\xi),\quad \tilde{\varphi}_j(\xi)=\sum_{i=0}^{4}a_{ij}(l+\xi)^{i/2}$$
$$a_{0j}\neq 0 \quad \text{if and only if } j=3,\quad a_{2j}=0\quad \forall j \tag{94}$$

see Appendix A. By defining $\mathbf{r}\overset{\text{def}}{=}\boldsymbol{\xi}-\boldsymbol{\eta}$ and $d_1=l+\eta_1$ as in Figure 20, it holds:

$$\sqrt{l+\xi_1}=\sqrt{d_1+r_1},\quad (l+\xi_1)^{3/2}=(d_1+r_1)\sqrt{d_1+r_1}$$

DOI: 10.1002/nme

and Equation (40) still applies. By a trivial variable change, Equation (42) becomes:

$$\mathbf{F}_{rs}(\mathbf{x}, T_{\text{tip}}) = \int_{-(\eta_1+l)}^{-(\eta_1-l)} \mathbf{G}_{rs}(-\mathbf{r}) \begin{bmatrix} \mathbf{r}_1^{\mathsf{T}} & 0 \\ 0 & \mathbf{r}_1^{\mathsf{T}} \end{bmatrix} \sqrt{d_1 + r_1}\, \mathrm{d}r_1 \Bigg|_{r_2=x_2} \begin{bmatrix} \mathbf{X}\mathbf{a}_n & 0 \\ 0 & \mathbf{X}\mathbf{a}_n \end{bmatrix} \tag{95}$$

and by noting that $\mathbf{G}_{up}(-\mathbf{r}) = -\mathbf{G}_{up}(\mathbf{r})$ and $\mathbf{G}_{pp}(-\mathbf{r}) = \mathbf{G}_{pp}(\mathbf{r})$ identities (44) and (45) still applies by suitably changing the integration interval for r_1. All obtained results extends straightforwardly.

Exploiting analytical integrations (45), an asymptotical analysis of the approximated stress field around the crack tip has been carried out. Starting from representation formula (6) for the stress field, formula (90) for the approximation of SIFs came out taking the limit to the crack tip of the approximated stress field. In this sense it can be stated that formula (90) is 'coherent with the approximated stress field', property that does not hold for all formulae for SIFs approximation (typically the J-integral or the 'one point formula').

From the computational side, analytical integrations seems to be of interest for their easy implementation and for their efficiency, especially in the surrounding zone emerged in Section 4.5. An object-oriented computer code, that implements the proposed integration schemes, has been developed and is available for the scientific community upon request. By means of it, numerical analysis for SIFs approximation have been performed over a set of academical examples and benchmarks. Further publications will be devoted to analysis of real-life engineering problems, with the aim of assessing the safety factors of structural brittle components.

The obtained results stimulate further work. It has been shown even in 3D that the interpolated crack opening displacement $\mathbf{w}(\mathbf{x})$ must comply with the asymptotic vanishing of the term that is linear in distance to the crack tip. Special shape functions must be devised to this aim. Extension of the proposed analysis to 3D may be useful in addressing the complicated problem of *accurate and efficient computational strategies for 3D SIFs evaluation*.

The accuracy obtained in SIFs approximation seems to have promising falls in the context of *Crack propagation*, because several criterions proposed in the literature are based on the approximation of SIFs. Together with contact algorithms to simulate crack closure effects, the propagation of brittle fractures in structural elements seems to be an affordable task especially for fatigue crack growth, which may take advantages of recently published variational approaches for crack initiation in hyperelastic bodies.

In more theoretical scenarios, the challenge in understanding fracture lies in the fact that several length scales are connected and all may contribute to fracture energy. Using the proposal accurate SIFs approximations as a numerical tool for multi-scale simulation of fracture from macroscopic to atomistic scale seems yet to produce very promising results, as from initial numerical analysis.

APPENDIX A: MODIFIED QUARTER POINT SHAPE FUNCTIONS

Approximation of opening and sliding $\mathbf{w}$ at the crack tip reads (see Equation (35)):

$$\mathbf{w}(\xi) = \sum_{j=0}^{2} \mathbf{w}_j \tilde{\varphi}_j(\xi), \quad \tilde{\varphi}_j(\xi) = \sum_{i=0}^{4} a_{ij}(l-\xi)^{i/2}$$

$$a_{0j} \neq 0 \quad \text{if and only if } j = 3, \quad a_{2j} = 0 \quad \forall j$$

DOI: 10.1002/nme

with $\xi \in [-l, l]$. Shape functions $\tilde{\varphi}_j(\xi)$ read in extenso:

$$\tilde{\varphi}_0(\xi) = \frac{\sqrt{2}}{11\sqrt{l}}\sqrt{l-\xi} - \frac{63\sqrt{2}}{88l^{3/2}}(l-\xi)^{3/2} + \frac{81}{88l^2}(l-\xi)^2$$

$$\tilde{\varphi}_1(\xi) = -\frac{27\sqrt{2}}{44\sqrt{l}}\sqrt{l-\xi} + \frac{351\sqrt{2}}{88l^{3/2}}(l-\xi)^{3/2} - \frac{81}{22l^2}(l-\xi)^2$$

$$\tilde{\varphi}_2(\xi) = \frac{27\sqrt{2}}{11\sqrt{l}}\sqrt{l-\xi} - \frac{513\sqrt{2}}{88l^{3/2}}(l-\xi)^{3/2} + \frac{405}{88l^2}(l-\xi)^2$$

$$\tilde{\varphi}_3(\xi) = 1 - \frac{85\sqrt{2}}{44\sqrt{l}}\sqrt{l-\xi} + \frac{225\sqrt{2}}{88l^{3/2}}(l-\xi)^{3/2} - \frac{81}{44l^2}(l-\xi)^2$$

If the crack tip is located at $\xi = -l$, shape functions, now denoted with $\tilde{\varsigma}_j(\xi)$ read:

$$\tilde{\varsigma}_0(\xi) = \tilde{\varphi}_3(-\xi)$$

$$\tilde{\varsigma}_1(\xi) = \tilde{\varphi}_2(-\xi)$$

$$\tilde{\varsigma}_2(\xi) = \tilde{\varphi}_1(-\xi)$$

$$\tilde{\varsigma}_3(\xi) = \tilde{\varphi}_0(-\xi)$$

APPENDIX B: LEBESGUE INTEGRALS

The following identities, that can be proved by induction when $r_2 \neq 0$, are the keynote of the inner integration. Here, $M_2[k]$ stands for the remainder of the (integer) division $k \div 2$.

$$\begin{aligned}\int_{x_1-l_j}^{x_1+l_j} r_1^k \log(r^2)\,\mathrm{d}r_1\bigg|_{r_2=x_2} = \Bigg[& \log(r_1^2+x_2^2)\left(\frac{r_1^{k+1}}{k+1} + M_2[k](-1)^{k-1/2}x_2^{k+1}\right) \\ & + \arctan\left(\frac{r_1}{x_2}\right)\left((1-M_2[k])\frac{2}{k-1}(-1)^{k/2}x_2^{k+1}\right) \\ & + r_1\sum_{n=0}^{k} M_2[k+1-n]\frac{2}{(k+1)(n+1)}(-1)^{((k-n)/2+1)}r_1^n x_2^{k-n}\Bigg]_{r_1=x_1-l_j}^{r_1=x_1+l_j}\end{aligned} \tag{B1}$$

DOI: 10.1002/nme

$$\int_{x_1-l_j}^{x_1+l_j} \frac{r_1^k}{r^2}\,\mathrm{d}r_1\bigg|_{r_2=x_2} = \Bigg[\log(r_1^2+x_2^2)(M_2[k](-1)^{k-1/2}x_2^{k-1}) + \arctan\left(\frac{r_1}{x_2}\right)((1-M_2[k])(-1)^{k/2}x_2^{k-1}) \times \sum_{n=1}^{k}\frac{M_2[k-n]}{n}(-1)^{((k-n+1)/2+1)}r_1^n x_2^{k-n-1}\Bigg]_{r_1=x_1-l_j}^{r_1=x_1+l_j} \tag{B2}$$

$$\int_{x_1-l_j}^{x_1+l_j} \frac{r_1^k}{r^4}\,\mathrm{d}r_1\bigg|_{r_2=x_2} = \Bigg[\frac{1}{2}\log(r_1^2+x_2^2)\left(-\frac{k-1}{2}M_2[k](-1)^{k-1/2}x_2^{k-3}\right) + \frac{1}{2}\arctan\left(\frac{r_1}{x_2}\right)\left((k-1)(M_2[k]-1)(-1)^{k/2}x_2^{k-3}\right) + \frac{1}{2}\frac{1}{r^2}x_2^{k-2}(-M_2[k](-1)^{k-1/2}x_2+(1-M_2[k])(-1)^{k/2}r_1) + \sum_{n=1}^{k-2}M_2[k-n]\frac{k-n-1}{2n}(-1)^{k-n+1/2}r_1^n x_2^{k-n-3}\Bigg]_{r_1=x_1-l_j}^{r_1=x_1+l_j} \tag{B3}$$

$$\int_{x_1-l_j}^{x_1+l_j} \frac{r_1^k}{r^6}\,\mathrm{d}r_1\bigg|_{r_2=x_2} = \Bigg[\frac{1}{4}\log(r_1^2+x_2^2)\left(\frac{k-3}{2}\frac{k-1}{2}M_2[k](-1)^{k-1/2}x_2^{k-5}\right) + \frac{1}{4}\arctan\left(\frac{r_1}{x_2}\right)\left(\frac{k-3}{2}(k-1)(1-M_2[k])(-1)^{k/2}x_2^{k-5}\right) + \frac{1}{4}\frac{1}{r^4}x_2^{k-2}(-M_2[k](-1)^{k-1/2}x_2+(1-M_2[k])(-1)^{k/2}r_1) + \frac{1}{4}\frac{1}{r^2}x_2^{k-4}\left(M_2[k](-1)^{k-1/2}(k-1)x_2 - (1-M_2[k])(-1)^{k/2}\frac{2k-3}{2}r_1\right) + \frac{1}{8}\sum_{n=1}^{k-4}M_2[k-n]\frac{k-n-1}{n}(k-n-3) \times (-1)^{(k-n-1)/2}r_1^n x_2^{k-n-5}\Bigg]_{r_1=x_1-l_j}^{r_1=x_1+l_j} \tag{B4}$$

DOI: 10.1002/nme

APPENDIX C: TABLES

In this appendix, tables $\mathbf{L}_{pp}$, $\mathbf{A}_{pp}$, $\mathbf{P}_{pp}$, $\mathbf{L}_{up}$, $\mathbf{A}_{up}$, and $\mathbf{P}_{up}$ for shape functions (38) are collected, denoting with: r_1 as in Equations (44)–(45), $\mathbf{d}=\{d_1, d_2\}$, $d_1 = l - \eta_1$, $\alpha = \sqrt{d_1 + r_1}$, and $d_2 = -\eta_2$ having defined $\eta_1 = \xi_1(\mathbf{x})$ and $\eta_2 = \xi_2(\mathbf{x})$ according to Figure 7. Define moreover functions $a : \mathbb{R}^2 \to \mathbb{R}$ and $b : \mathbb{R}^2 \to \mathbb{R}$ as follows:

$$a(\mathbf{d}) = \frac{\sqrt{|\mathbf{d}| + d_1}}{\sqrt{2}}, \quad b(\mathbf{d}) = -\mathrm{sgn}(d_2)\frac{\sqrt{|\mathbf{d}| - d_1}}{\sqrt{2}} \tag{C1}$$

C.1. Strongly singular kernel $\mathbf{G}_{up}$

$$\mathbf{L}_{up}[1,1] = \left\{ \frac{3d_2}{|\mathbf{d}|}a(\mathbf{d}) + 2b(\mathbf{d})\left(-1+2v+\frac{d_1}{|\mathbf{d}|}\right), -\frac{5{d_2}^2}{|\mathbf{d}|}b(\mathbf{d}) - \frac{d_2(-4d_1+2|\mathbf{d}|(-1+2v))}{|\mathbf{d}|}a(\mathbf{d}) \right\}$$

$$\mathbf{L}_{up}[1,2] = \left\{ 2a(\mathbf{d})(1-2v) - b(\mathbf{d})\frac{d_2}{|\mathbf{d}|}, -\frac{3{d_2}^2}{|\mathbf{d}|}a(\mathbf{d}) - \frac{2d_2(d_1 + |\mathbf{d}|(-1+2v))}{|\mathbf{d}|}b(\mathbf{d}) \right\}$$

$$\mathbf{L}_{up}[2,1] = \left\{ 2a(\mathbf{d})(-1+2v) - b(\mathbf{d})\frac{d_2}{|\mathbf{d}|}, -\frac{3{d_2}^2}{|\mathbf{d}|}a(\mathbf{d}) - \frac{2d_2(d_1 + |\mathbf{d}|(1-2v))}{|\mathbf{d}|}b(\mathbf{d}) \right\}$$

$$\mathbf{L}_{up}[2,2] = \left\{ a(\mathbf{d})\frac{d_2}{|\mathbf{d}|} + 2b(\mathbf{d})\left(-1+2v+\frac{d_1}{|\mathbf{d}|}\right), \frac{{d_2}^2}{|\mathbf{d}|}b(\mathbf{d}) + a(\mathbf{d})d_2(2-4v) \right\}$$

$$\mathbf{A}_{up}[1,1] = \left\{ -b(\mathbf{d})\frac{6d_2}{|\mathbf{d}|} + 4a(\mathbf{d})\frac{(d_1+(1-2v)|\mathbf{d}|)}{|\mathbf{d}|}, -\frac{10{d_2}^2}{|\mathbf{d}|}a(\mathbf{d}) - \frac{2d_2(4d_1+2|\mathbf{d}|(-1+2v))}{|\mathbf{d}|}b(\mathbf{d}) \right\}$$

$$\mathbf{A}_{up}[1,2] = \left\{ b(\mathbf{d})(4-8v) - 2a(\mathbf{d})\frac{d_2}{|\mathbf{d}|}, \frac{6{d_2}^2}{|\mathbf{d}|}b(\mathbf{d}) + \frac{2d_2(-2d_1 + 2|\mathbf{d}|(-1+2v))}{|\mathbf{d}|}a(\mathbf{d}) \right\}$$

$$\mathbf{A}_{up}[2,1] = \left\{ b(\mathbf{d})(-4+8v) - 2a(\mathbf{d})\frac{d_2}{|\mathbf{d}|}, \frac{6{d_2}^2}{|\mathbf{d}|}b(\mathbf{d}) - \frac{4d_2(d_1 + |\mathbf{d}|(-1+2v))}{|\mathbf{d}|}a(\mathbf{d}) \right\}$$

$$\mathbf{A}_{up}[2,2] = \left\{ -2b(\mathbf{d})\frac{d_2}{|\mathbf{d}|} + 4a(\mathbf{d})\frac{(d_1 + (1-2v)|\mathbf{d}|)}{|\mathbf{d}|}, \frac{2{d_2}^2}{|\mathbf{d}|}a(\mathbf{d}) + 2b(\mathbf{d})d_2(2-4v) \right\}$$

$$\mathbf{S}_{up}[1,1] = \{4r_1 d_2, -4{d_2}^3\}$$

$$\mathbf{S}_{up}[1,2] = \{-4\,d_2^2, -4r_1\,d_2^2\}$$

$$\mathbf{S}_{up}[2,1] = \{-4\,d_2^2, -4r_1\,d_2^2\}$$

$$\mathbf{S}_{up}[2,2] = \{-4r_1 d_2, 4{d_2}^3\}$$

DOI: 10.1002/nme

$$\mathbf{P}_{up}[1,1] = \{0, 4d_2(-6+4\nu)\}$$

$$\mathbf{P}_{up}[1,2] = \{8(-1+2\nu), \tfrac{4}{3}(2(d_1+r_1)(2\nu-1))\}$$

$$\mathbf{P}_{up}[2,1] = \{8(1-2\nu), \tfrac{4}{3}(-2(d_1+r_1)(2\nu-1))\}$$

$$\mathbf{P}_{up}[2,2] = \{0, 4d_2(-2+4\nu)\}$$

C.2. Hypersingular kernel

$$\begin{aligned}\mathbf{L}_{pp}[1,1] = \Bigg\{ & -\frac{a(\mathbf{d})}{|\mathbf{d}|^3}[-d_1d_2n_1+2{d_1}^2n_2(-1+4\nu)+{d_2}^2n_2(-3+8\nu)] \\ & -\frac{b(\mathbf{d})}{d_2|\mathbf{d}|^3}[-4\,{d_1}^2\,(-d_2n_1+|\mathbf{d}|n_2(1-2\nu))+4{d_1}^3n_2(-1+2\nu) \\ & +d_1{d_2}^2n_2(-3+8\nu)+{d_2}^2(3d_2n_1+4|\mathbf{d}|n_2(-1+2\nu))], \\ & \frac{b(\mathbf{d})}{|\mathbf{d}|^3}[-8d_1^3n_1+2d_1^2d_2n_2(3+4\nu)-9d_1d_2^2n_1+n_2(5+8\nu)d_2^3] \\ & +\frac{a(\mathbf{d})}{|\mathbf{d}|^3}[-8d_1^3n_2\nu-16d_1^2d_2n_1-d_1d_2^2n_2(1+8\nu)-15n_1d_2^3+4n_2(-1+2\nu)|\mathbf{d}|^3]\Bigg\}\end{aligned}$$

$$\begin{aligned}\mathbf{L}_{pp}[1,2] = \Bigg\{ & \frac{a(\mathbf{d})}{|\mathbf{d}|^3}[2{d_1}^2n_1+3{d_2}^2n_1-d_1d_2n_2] \\ & -\frac{b(\mathbf{d})}{d_2|\mathbf{d}|^3}[-4{d_1}^3n_1-3d_1{d_2}^2n_1-4{d_1}^2|\mathbf{d}|n_1-{d_2}^2(4|\mathbf{d}|n_1-d_2n_2)], \\ & \frac{b(\mathbf{d})}{|\mathbf{d}|^3}d_2[6d_1^2n_1+d_1d_2n_2+5n_1d_2^2]+\frac{a(\mathbf{d})}{|\mathbf{d}|^3}[-d_1d_2^2n_1+4d_1^2d_2n_2+3d_2^3n_2-4n_1|\mathbf{d}|^3]\Bigg\}\end{aligned}$$

$$\mathbf{L}_{pp}[2,1] = \mathbf{L}_{pp}[1,2]$$

$$\begin{aligned}\mathbf{L}_{pp}[2,2] = \Bigg\{ & \frac{a(\mathbf{d})}{|\mathbf{d}|^3}[-(d_1d_2n_1)+{d_2}^2n_2(9-8\nu)+2{d_1}^2n_2(5-4\nu)] \\ & -\frac{b(\mathbf{d})}{d_2|\mathbf{d}|^3}[-({d_2}^2(-d_2n_1+4|\mathbf{d}|n_2(3-2\nu)))+4{d_1}^3n_2(-3+2\nu) \\ & +4{d_1}^2|\mathbf{d}|n_2(-3+2\nu)+d_1{d_2}^2n_2(-13+8\nu)], \\ & -\frac{b(\mathbf{d})}{|\mathbf{d}|^3}d_2[2d_1^2n_2(5-4\nu)-d_1n_1d_2+n_2(9-8\nu)d_2^2] \\ & +\frac{a(\mathbf{d})}{|\mathbf{d}|^3}[8d_1^3n_2(1-\nu)+4d_1^2n_1d_2+d_1n_2(9-8\nu)d_2^2+3n_1d_2^3-4n_2(3-2\nu)|\mathbf{d}|^3]\Bigg\}\end{aligned}$$

DOI: 10.1002/nme

$$\mathbf{S}_{pp}[1,1]=\left\{\frac{4(-(d_1d_2(-(d_2n_2)+n_1r_1))+{d_2}^2(-7d_2n_1-3n_2r_1)+{d_1}^2(-6d_2n_1-2n_2r_1))}{|\mathbf{d}|^2},\right.$$

$$\left.-4d_2\frac{8{d_1}^2(-d_2n_2+n_1r_1)+9{d_2}^2(-d_2n_2+n_1r_1)-d_1d_2(d_2n_1+n_2r_1)}{|\mathbf{d}|^2}\right\}$$

$$\mathbf{S}_{pp}[1,2]=\left\{\frac{-4(2{d_1}^2(-(d_2n_2)+n_1r_1)+3{d_2}^2(-(d_2n_2)+n_1r_1)-d_1d_2(d_2n_1+n_2r_1))}{|\mathbf{d}|^2},\right.$$

$$\left.-4d_2\frac{-d_1d_2(-d_2n_2+n_1r_1)+{d_2}^2(-9d_2n_1-5n_2r_1)+{d_1}^2(-8d_2n_1-4n_2r_1)}{|\mathbf{d}|^2}\right\}$$

$$\mathbf{S}_{pp}[2,1]=\mathbf{S}_{pp}[1,2]$$

$$\mathbf{S}_{pp}[2,2]=\left\{\frac{-4(-(d_1d_2(-(d_2n_2)+n_1r_1))+{d_2}^2(-3d_2n_1+n_2r_1)+2{d_1}^2(-(d_2n_1)+n_2r_1))}{|\mathbf{d}|^2},\right.$$

$$\left.4d_2\frac{4{d_1}^2(-d_2n_2+n_1r_1)+5{d_2}^2(-d_2n_2+n_1r_1)-d_1d_2(d_2n_1+n_2r_1)}{|\mathbf{d}|^2}\right\}$$

$$\mathbf{H}_{pp}[1,1]=\{16{d_2}^2(d_2n_1+n_2r_1),\,16{d_2}^3(-d_2n_2+n_1r_1)\}$$

$$\mathbf{H}_{pp}[1,2]=\{16{d_2}^2(-d_2n_2+n_1r_1),\,16{d_2}^3(-d_2n_1-n_2r_1)\}$$

$$\mathbf{H}_{pp}[2,1]=\mathbf{H}_{pp}[1,2]$$

$$\mathbf{H}_{pp}[2,2]=\{-16{d_2}^2(d_2n_1+n_2r_1),\,-16{d_2}^3(-d_2n_2+n_1r_1)\}$$

$$\mathbf{A}_{pp}[1,1]=\left\{2\frac{b(\mathbf{d})}{|\mathbf{d}|^3}[-(d_1d_2n_1)+2{d_1}^2n_2(-1+4v)+{d_2}^2n_2(-3+8v)]\right.$$

$$+2\frac{a(\mathbf{d})}{d_2|\mathbf{d}|^3}[d_1{d_2}^2n_2(3-8v)+{d_1}^3n_2(4-8v)$$

$$+4{d_1}^2(-(d_2n_1)+|\mathbf{d}|n_2(-1+2v))+{d_2}^2(-3d_2n_1+4|\mathbf{d}|n_2(-1+2v))],$$

$$-2\frac{a(\mathbf{d})}{|\mathbf{d}|^3}[8d_1^3n_1-2d_1^2d_2n_2(3+4v)+9d_1n_1d_2^2-n_2(5+8v)d_2^3]$$

$$\left.-2\frac{b(\mathbf{d})}{|\mathbf{d}|^3}[-8d_1^3n_2v-16d_1^2n_1d_2-d_1n_2(1+8v)d_2^2-15n_1d_2^3+4n_2(1-2v)|\mathbf{d}|^3]\right\}$$

DOI: 10.1002/nme

$$\mathbf{A}_{pp}[1,2]=\left\{-2\frac{b(\mathbf{d})}{|\mathbf{d}|^3}[2{d_1}^2n_1+3{d_2}^2n_1-d_1d_2n_2]\right.$$

$$-\frac{a(\mathbf{d})}{d_2|\mathbf{d}|^3}[-8{d_1}^3n_1-6d_1{d_2}^2n_1+8{d_1}^2|\mathbf{d}|n_1+8{d_2}^2|\mathbf{d}|n_1+2{d_2}^3n_2],$$

$$-2\frac{a(\mathbf{d})}{|\mathbf{d}|^3}d_2[-6d_1^2n_1-d_1n_2d_2-5n_1d_2^2]$$

$$\left.+2\frac{b(\mathbf{d})}{|\mathbf{d}|^3}[-4d_1^2n_2d_2+d_1n_1d_2^2-3n_2d_2^3-4n_1|\mathbf{d}|^3]\right\}$$

$$\mathbf{A}_{pp}[2,1]=\mathbf{A}_{pp}[1,2]$$

$$\mathbf{A}_{pp}[2,2]=\left\{-2\frac{b(\mathbf{d})}{|\mathbf{d}|^3}[-(d_1d_2n_1)+{d_2}^2n_2(9-8\nu)+2{d_1}^2n_2(5-4\nu)]\right.$$

$$+2\frac{a(\mathbf{d})}{d_2|\mathbf{d}|^3}[d_1{d_2}^2n_2(13-8\nu)+4{d_1}^3n_2(3-2\nu)$$

$$+4{d_1}^2|\mathbf{d}|n_2(-3+2\nu)+{d_2}^2(-(d_2n_1)+4|\mathbf{d}|n_2(-3+2\nu))],$$

$$-2\frac{a(\mathbf{d})}{|\mathbf{d}|^3}d_2[2d_1^2n_2(5-4\nu)-d_1n_1d_2+n_2(9-8\nu)d_2^2]$$

$$+2\frac{b(\mathbf{d})}{|\mathbf{d}|^3}[8d_1^3n_2(-1+\nu)-4d_1^2n_1d_2+d_1n_2(-9+8\nu)d_2^2$$

$$\left.-\ 3n_1d_2^3-4n_2(3-2\nu)|\mathbf{d}|^3]\right\}$$

$$\mathbf{P}_{pp}[1,1]=\{0,16\,n_2\}$$

$$\mathbf{P}_{pp}[1,2]=\{0,16\,n_1\}$$

$$\mathbf{P}_{pp}[2,1]=\mathbf{P}_{pp}[1,2]$$

$$\mathbf{P}_{pp}[2,2]=\{0,16\,n_2\}$$

ACKNOWLEDGEMENTS

The support of the Italian Ministry of University and Research (MIUR) under grant ex 60%—2005: 'Analisi non lineari nella meccanica dei continui e della frattura mediante il metodo degli elementi al contorno' is gratefully acknowledged.

DOI: 10.1002/nme

REFERENCES

1. McLean W. *Strongly Elliptic Systems and Boundary Integral Equations*. Cambridge University Press: New York, 2000.
2. Aliabadi MH. Boundary element formulations in fracture mechanics. *Applied Mechanical Review* 1997; **50**:83–96.
3. Salvadori A. A symmetric boundary integral formulation for cohesive interface problems. *Computational Mechanics* 2003; **32**(4–6):381–391.
4. Aliabadi MH, Brebbia CA, Parton VZ. *Static and Dynamic Fracture Mechanics*. Computational Mechanics Publications: Southampton, Boston, 1994.
5. Brebbia CA, Telles JCF, Wrobel LC. *Boundary Element Techniques*. Springer: Berlin, 1984.
6. Salvadori A. Analytical integrations in 2D BEM elasticity. *International Journal for Numerical Methods in Engineering* 2002; **53**(7):1695–1719.
7. Hong KH, Chen JT. Derivations of integral equations of elasticity. *Journal of Engineering Mechanics* (ASCE) 1988; **114**:1028–1044.
8. Sirtori S, Maier G, Novati G, Miccoli S. A Galerkin symmetric boundary-element method in elasticity: formulation and implementation. *International Journal for Numerical Methods in Engineering* 1992; **35**:255–282.
9. Diligenti M, Monegato G. Finite-part integrals, their occurrence and computation. *Rend. Circ. Mat. Palermo* 1993; **33**(II):39–61.
10. Mantič V. On computing boundary limiting values of boundary integrals with strongly singular and hypersingular kernels in 3D BEM for elastostatics. *Engineering Analysis with Boundary Elements* 1994; **13**:115–134.
11. Guiggiani M. Formulation and numerical treatment of boundary integral equations with hypersingular kernels. In *Singular Integrals in Boundary Element Methods*, Sladek V, Sladek J (eds). Advances in Boundary Elements Series. Computational Mechanics Publications: Southampton, Boston, 1998; 85–124.
12. Hadamard J. *Lectures on Cauchy's Problem in Linear Partial Differential Equations*. Yale University Press: New Haven, Conn., U.S.A., 1923.
13. Krishnasamy G, Rizzo FJ, Rudolphi TJ. Hypersingular boundary integral equations: their occurrence, interpretation, regularization and computation. In *Developments in Boundary Element Methods*, Banerjee PK, Kobayashi S (eds). Elsevier Applied Science Publishers: Amsterdam, 1991.
14. Toh K, Mukherjee S. Hypersingular and finite part integrals in the boundary element method. *International Journal of Solids and Structures* 1994; **31**:2299–2312.
15. Mantič V. A new formula for the *c*-matrix in the Somigliana identity. *Journal of Elasticity* 1993; **33**:191–201.
16. Hartmann F. The somigliana identity on a piecewise smooth surface. *Journal of Elasticity* 1981; **11**:403–423.
17. Guiggiani M. Hypersingular boundary integral equations have an additional free term. *Computational Mechanics* 1995; **16**:245–248.
18. Mantič V, Paris F. Existence and evaluation of the two free terms in the hypersingular boundary integral equation of potential theory. *Engineering Analysis with Boundary Elements* 1995; **16**:253–260.
19. Salvadori A. Analytical integrations in 2D BEM fracture mechanics. *Technical Report*, Quaderni del Seminario Matematico di Brescia, 2005.
20. Bonnet M, Maier G, Polizzotto C. Symmetric Galerkin boundary element method. *Applied Mechanical Review* 1998; **51**:669–704.
21. Cruse TA. *Boundary Element Analysis in Computational Fracture Mechanics*. Kluwer Academic: Dordrecht, The Netherlands, 1988.
22. Aliabadi MH, Rooke DP. *Numerical Fracture Mechanics*. Kluwer Academic: Dordrecht, 1991.
23. Cruse TA. Computational applications in applied mechanics. ASME: New York, 1975; 31–46.
24. Ligget JA, Liu PLF. *The Boundary Integral Equation Method for Porous Media Flow*. Allen & Unwin: London, 1983.
25. Portela A, Aliabadi MH, Rooke DP. The dual boundary element method: effective implementations for crack problems. *International Journal for Numerical Methods in Engineering* 1992; **33**:1269–1287.
26. Rice J. Mathematical analysis in the mechanics of fracture. In *Fracture—An Advanced Treatise*, Liebowitz J (ed.), vol. 2. Pergamon Press: Oxford, 1968; 191–311.
27. Williams ML. On the stress distribution at the base of a stationary crack. *Journal of Applied Mechanics* (ASME) **24**:109–114.
28. Henshell RD, Shaw KG. Crack tip finite elements are unnecessary. *International Journal for Numerical Methods in Engineering* 1975; **9**:495–507.
29. Barsoum RS. On the use of isoparametric finite elements in linear fracture mechanics. *International Journal for Numerical Methods in Engineering* 1976; **10**:25–37.

DOI: 10.1002/nme

30. Gray LJ, Paulino GH. Crack tip interpolation, revisited. *SIAM Journal on Applied Mathematics* 1998; **58**:428–455.
31. Gray LJ, Phan AV, Paulino GH, Kaplan T. Improved quarter point crack tip element. *Engineering Fracture Mechanics* 2003; **70**:269–283.
32. Kane JH, Balakrishna C. Symmetric Galerkin boundary formulations employing curved elements. *International Journal for Numerical Methods in Engineering* 1993; **36**:2157–2187.
33. Rudolphi TJ. The use of simple solutions in the regularization of hypersingular boundary integral equations. *Mathematical and Computer Modelling* 1991; **15**:269–278.
34. Bonnet M. A regularized Galerkin symmetric BIE formulation for mixed 3D elastic boundary values problems. *Boundary Elements Abstracts and Newsletters* 1993; **4**:109–113.
35. Sladek J, Sladek V. Transient elastodynamic three dimensional problems in cracked bodies. *Applied Mathematical Modelling* 1984; **8**:2–10.
36. Kutt HR. The numerical evaluation of principal value integrals by finite-part integration. *Numerische Mathematik* 1975; **24**:205–210.
37. Elliott D, Paget DF. Gauss type quadrature rules for Cauchy principal value integrals. *Mathematics of Computation* 1979; **33**(145):301–309.
38. Monegato G. The numerical evaluation of hypersingular integrals. *Journal of Computational and Applied Mathematics* 1994; **50**:9–31.
39. Hui CY, Shia D. Evaluations of hypersingular integrals using Gaussian quadrature. *International Journal for Numerical Methods in Engineering* 1999; **44**:205–214.
40. Holzer S. How to deal with hypersingular integrals in the symmetric BEM. *Communications in Applied Numerical Methods* 1993; **9**:219–232.
41. Balakrishna C, Gray LJ, Kane JH. Efficient analytic integration of symmetric Galerkin boundary integrals over curved elements, thermal conduction formulation. *Computer Methods in Applied Mechanics and Engineering* 1994; **111**:335–355.
42. Gray LJ, Martha LF, Ingraffea AR. Hypersingular integrals in boundary element fracture analysis. *International Journal for Numerical Methods in Engineering* 1990; **29**:1135–1158.
43. Gray JL, Soucie SC. A hermite interpolation algorithm for hypersingular boundary integrals. *International Journal for Numerical Methods in Engineering* 1993; **36**:2357–2367.
44. Carini A, Salvadori A. Analytical integrations in 3D BEM: preliminaries. *Computational Mechanics* 2002; **28**(3–4):177–185.
45. Westergaard HM. Bearing pressures and cracks. *Journal of Applied Mechanics* 1939; **6**:49–53.
46. Zemanian AH. *Distribution Theory and Transform Analysis*. Dover: New York, 1987.
47. Guiggiani M. Hypersingular formulation for boundary stress evaluation. *Engineering Analysis with Boundary Elements* 1994; **13**:169–179.
48. Schwab C, Wendland WL. Kernel properties and representations of boundary integral operators. *Mathematische Nachrichten* 1992; **156**:187–218.
49. Aliabadi MH. A new generation of boundary element methods in fracture mechanics. *International Journal of Fracture* 1997; **86**:91–125.
50. Yau JF, Wang SS, Corten HT. A mixed-mode crack analysis of isotropic solids using conservation laws of elasticity. *Journal of Applied Mechanics* 1980; **47**:335–341.
51. Blandford GE, Ingraffea A, Liggett JA. Two-dimensional stress intensity factor computations using the boundary element method. *International Journal for Numerical Methods in Engineering* 1981; **17**:387–404.
52. Martinez J, Dominguez J. On the use of quarter point boundary elements for stress intensity factor computations. *International Journal for Numerical Methods in Engineering* 1984; **20**:1941–1950.
53. Murakami Y (ed.). *Stress Intensity Factors Handbook*. Pergamon Press: Oxford, 2003.

DOI: 10.1002/nme